

---

# Effectiveness of Vision Language Models for Open-world Single Image Test Time Adaptation

---

Manogna Sreenivas, Soma Biswas  
Indian Institute of Science  
Bengaluru, India  
{manognas, somabiswas}@iisc.ac.in

## Abstract

We propose a novel framework to address the real-world challenging task of Single Image Test Time Adaptation in an open and dynamic environment. We leverage large scale Vision Language Models like CLIP to enable real time adaptation on a per-image basis without access to source data or ground truth labels. Since the deployed model can also encounter unseen classes in an open world, we first employ a simple and effective Out of Distribution (OOD) detection module to distinguish between weak and strong OOD samples. We propose a novel contrastive learning based objective to enhance the discriminability between weak and strong OOD samples by utilizing small, dynamically updated feature banks. Finally, we also employ a classification objective for adapting the model using the reliable weak OOD samples. The proposed framework **ROSITA** combines these components, enabling continuous online adaptation of Vision Language Models on a single image basis. Extensive experimentation on diverse domain adaptation benchmarks validates the effectiveness of the proposed framework. Our code can be found at the project site <https://manogna-s.github.io/rosita/>

## 1 Introduction

Over the past decade, substantial advancements have been achieved in various computer vision tasks [1, 2, 3, 4]. However, these achievements are predominantly realized under the assumption that both training and test data originate from the same distribution. In contrast, the real world is dynamic and ever-changing, making such assumptions often untenable. Distribution gaps between training and test data manifest in diverse forms [5, 6], including domain shifts and semantic shifts. Domain shifts emerge from variations in lighting, weather, camera specifications, or geographical locations between the train and test datasets. Semantic shifts occur when a model, initially trained on a specific set of classes, encounters previously unseen classes during testing. Navigating deep learning models through these dynamic test environments is hence imperative.

Researchers have been tackling the robustness of models facing domain shifts, diving into paradigms like Unsupervised Domain Adaptation [7, 8, 9], Source-Free Domain Adaptation [10, 11, 12, 13] and more recently, the problem of Test Time Adaptation (TTA) [14, 15, 16] has come to the forefront. TTA is characterized with three key factors: (1) No access to source data; (2) No ground truth labels for test data; (3) An online adaptation scenario where the model encounters test samples only once, reflecting the online nature of real-world. Several TTA methods [14, 10, 17, 18] address these challenges by minimizing self-training objectives. A more realistic and challenging setting is that of Continuous Test Time Adaptation (CTTA) [19, 20, 21] where the test domains change with time.

Another facet of distribution gaps lies in semantic shifts [22, 23]. While TTA methods have predominantly focused on closed-set scenarios, the real world seldom operates within such constraints. A classic example is that of autonomous driving, where models trained for specific geographical loca-

tions are deployed elsewhere. The vehicle might encounter new road signs, markings, or infrastructure not part of its training set. In this new environment, the model must categorize unfamiliar elements as unseen classes, rather than misclassifying them into known categories. This drives the need for Open world learning. Only recently, this has been explored in TTA setting in [22, 23]. However, these TTA/CTTA methods [14, 17, 23, 22] typically require *a batch of images* to be accumulated for model updates, which may not be feasible in real scenarios where test samples arrive individually. This highlights the need for effective Single Image Test Time Adaptation methods.

In this work, we address these two real world challenges through the proposed **Robust Open world Single Image Test time Adaptation (ROSITA)** framework. Parallel to the recent advances in TTA, there has been tremendous progress in the development of large scale Vision Language Models (VLM) like CLIP [24]. Having trained on large scale web scrapped image-text pairs, these VLMs [24] have demonstrated impressive zero shot generalization capabilities. CLIP representations enable good zero shot evaluation and only recently, [25, 26] have shown that these VLMs can indeed be further adapted on each image during inference, further improving the zero shot generalization performance. *In this work, we leverage VLMs to enable the detection of samples from unseen classes, while also continuously adapting the model to domain shifts in real-time, processing one image at a time.*

Unlike prior works [23, 22] where the model is trained only on known classes, pretrained VLMs like CLIP are trained on large scale image-text pairs from the web, but not specifically on samples from these known classes. In the context of VLMs, we clarify that the term *known classes* refers to the classes which are of our interest, for which the text classifier is obtained from class names. Any other class which is not of our interest is termed an *unknown class*. With a slight abuse of terminology, we borrow the terms known and unknown classes from the literature in open world learning [23, 22, 27] for the ease of explanation. We refer to the test samples from known classes (of interest) with domain shift as weak OOD samples and those from unknown classes (not of interest) as strong OOD samples. CLIP based OOD detection has only been recently explored in [27] where they utilize known and unknown class data to train learnable "no" prompts in an offline manner. Ours is a more challenging problem where we need to equip CLIP with this ability to say "I don't know" in an online manner.

To this end, we first establish baselines by adapting the recent test time prompt tuning methods [25, 26] for VLMs in the test scenario where both weak and strong OOD samples arrive in an online manner. In such a scenario, it is necessary to filter the strong OOD samples, preventing it from corrupting the model during TTA. We use an LDA [28, 22] based OOD discriminator to identify a test sample as weak or strong OOD sample. Inorder to enhance the distinction between these two OOD samples, we propose a neighbourhood based clustering objective by leveraging two dynamically updating weak and strong OOD feature banks. Further, to aid the closed set classification accuracy of the weak OOD samples, we use pseudo label loss on reliable weak OOD samples, the reliability of a sample being determined based on its OOD score. To summarize, our contributions are as follows:

- To the best of our knowledge, this is the first work which addresses the realistic and challenging problem of open-world single image test time adaptation using VLMs.
- Analysis of the feasibility of continuous adaptation of VLMs during test time using single images and the choice of parameter group to update.
- A simple and efficient way to leverage the detected weak and strong OOD samples by utilizing a feature bank. The proposed objective improves the contrast between weak and strong OOD samples, thereby facilitating model adaptation while equipping it with the ability to say "I don't know".
- We demonstrate the effectiveness of our method by conducting extensive experiments on a wide variety of domain adaptation benchmarks, mimicking several real open world environments including single domain TTA, a more challenging Continual TTA scenario and varying the ratio of weak and strong OOD samples.

## 2 Preliminaries

Test time adaptation methods using CNNs [14, 15, 10, 17] successfully leverage test domain data arriving in an online manner (in batches) to continuously update the model. In this work, we study TTA of VLMs like CLIP, which has only been explored very recently [25, 26] by adapting prompts. While these methods [25, 26] show promise for on the fly adaptation in a zero-shot adaptation framework, it is not clear whether these frameworks can leverage the online data stream to

continuously update the model parameters as done in most TTA methods [14, 17]. In this work, we show that continuous adaptation of VLMs can indeed be helpful for online TTA. Here, we briefly discuss VLMs [24, 29] and the recent prompt tuning based TTA methods [25, 26], which we adapt as baselines here. Then, we present our analysis on the continuous adaptation of VLMs. Next, we formalize the problem statement and describe the proposed framework in detail.

## 2.1 Vision Language Models

**CLIP** [24] is a multimodal VLM consisting of two modules: Vision encoder and Text encoder denoted as  $\mathcal{F}_V$  and  $\mathcal{F}_T$  respectively. During pre-training, the two modules are jointly trained in a contrastive self-supervised fashion to align massive amounts of web scrapped image-text pairs. CLIP has demonstrated impressive zero-shot generalization ability across a wide variety of datasets.

**MaPLE** [29] is a multimodal prompt learner model that simultaneously adapts both the vision and text encoders while finetuning CLIP for downstream tasks. They use learnable text prompts  $\mathbf{p}_T$  and bridge the two modalities using visual prompts obtained as  $\mathbf{p}_V = \text{Proj}(\mathbf{p}_T)$ . Learnable tokens are also introduced in the deeper layers of both image and text encoders, to enable progressive adaptation of the features. As in [26], we use MaPLE as an additional VLM backbone to test our approach. We now review the baselines developed based on CLIP and MaPLE for zero-shot evaluation.

**ZSEval:** Given a test image  $x_t$ , the image feature is extracted from the vision encoder as  $f_t = \mathcal{F}_V(x_t)$ . For a  $C$ -class classification problem, the classifier is obtained by prepending a predefined text prompt  $\mathbf{p}_T = \text{"A photo of a"}$ , with the class names  $\{c_1, c_2, \dots, c_C\}$  to form class specific text inputs  $\{\mathbf{p}_T, c_i\}$  for  $i \in \{1, \dots, C\}$ . These texts are then embedded through the text encoder as  $\mathbf{t}_i = \mathcal{F}_T(\{\mathbf{p}_T; c_i\})$  to get the text classifiers  $\{\mathbf{t}_1, \mathbf{t}_2, \dots, \mathbf{t}_C\}$ . The class prediction is made by identifying the text feature  $\mathbf{t}_i$  which has the highest similarity with the image feature  $f_t$ .

**TPT** [25] aims to improve the zero shot generalization ability of CLIP by providing custom adaptable context for each image. This is done by prepending learnable text prompts  $\mathbf{p}_T$  to the class names instead of a predefined text prompt. The text classifiers  $\mathbf{t}_i = \mathcal{F}_T(\{\mathbf{p}_T; c_i\}), i \in \{1, 2, \dots, C\}$  are now a function of these learnable prompts, which are specially adapted for each test image using an entropy minimization objective as  $\arg \min_{\mathbf{p}_T} \mathcal{L}_{\text{ent}}$ . The entropy is obtained using the average score vector of the filtered augmented views.

**PromptAlign** [26] (**PAlign**) leverages multimodal prompt learner model MaPLE [29] to facilitate the adaptation of both vision and language encoders for each test sample. Inspired by earlier TTA works [15, 14], they propose to align the token distributions of source and target domains, considering ImageNet as a proxy for the source dataset of CLIP. The vision and language prompts of MaPLE are optimized with the objective  $\arg \min_{\{\mathbf{p}_V, \mathbf{p}_T\}} \mathcal{L}_{\text{ent}} + \mathcal{L}_{\text{align}}$  for each sample  $x_t$ .

**TPT-C/PAlign-C:** We adapt TPT and PAlign for continuous model update, which we refer as TPT-C and PAlign-C respectively. The prompts  $\{\mathbf{p}_T\}$  and  $\{\mathbf{p}_V, \mathbf{p}_T\}$  in TPT and PAlign are continuously updated with the test stream with their respective test objectives for this purpose.

## 2.2 Preliminary Analysis: Continuous adaptation of VLMs

While prompt tuning based methods [25, 26] have shown promise to improve the zero-shot generalization of VLMs, they do not continuously update the model in an online manner. They perform single image update, always starting from the base model. Based on the prior TTA works [14, 17], we analyse two aspects of VLMs for TTA task: (i) It is well established that continuous adaptation using test batches can mitigate the adverse effects of domain shift and improve model performance of CNNs [14, 17] during test time. In this work, we question if VLMs can be continuously adapted in a similar manner, but using only a single test image at a time?; (ii) If so, are prompts [25, 26] the best choice of parameters for continuous update?

**Experiment.** We choose three different parameter groups, namely, (1) Prompts [25, 26], (2) LayerNorm parameters [30], (3) Full network. We perform single image TTA in a closed set scenario on CIFAR-10C, by continuously adapting each of these parameter groups of CLIP, using entropy loss,  $L_{TTA} = \mathbb{1}(s_t > \tau) \mathcal{L}_{\text{ent}}(x_t)$  on reliable test samples, which is commonly used in several TTA methods [14, 16] and also recent VLM based prompt tuning methods [25, 26]. Here,  $x_t$  and  $s_t$  refer to the test sample and its confidence respectively.  $\tau$  is the confidence threshold used to select reliable samples [16] for the model update, which we set to 0.7 in all the experiments reported here.

**Observations.** We find that continuous model adaptation can indeed improve VLMs performance. Based on this empirical analysis (Figure 1), we find the LayerNorm parameters of the Vision encoder to be the best choice for single image test time tuning in terms of the performance and complexity.

Using a high learning rate of  $10^{-2}$  for any parameter group results in a severe drop in accuracy compared to the zero-shot performance of CLIP in this extreme setting of continuous single image model update. The other extreme of low learning rate of  $10^{-6}$  performs at par with ZSEval for Prompts and LayerNorm parameters, suggesting the model has not sufficiently changed to have an impact. Updating the Full Network results in an accuracy of about 10% across all learning rates, suggesting that giving the highest flexibility can even cause the model to lose the inherent generalization ability of the large scale VLM. LayerNorm parameters constitute only about 0.032% of the total CLIP parameters and we find this to be the right balance in terms of the flexibility given for the model to adapt to new domains, while also preserving the zero-shot generalization ability of CLIP. Our observation also complies with that in [30]

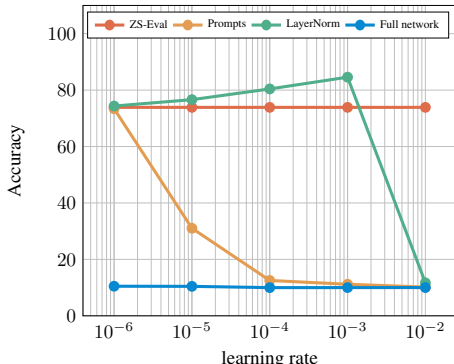


Figure 1: Accuracy on fine-tuning different parameter groups for single image TTA.

Most of the existing TTA approaches [15, 14, 17, 31] adjust the image representations for domain shifts during test time while keeping the classifiers fixed. This is done to retain the class discriminative information. In contrast, in TPT [25] and PAlign [26], the text based classifiers (which are a function of learnable prompts) are being updated based on a single image, which can be an outlier at times. This does not affect the zero-shot evaluation (when the model is reset after every image), but can be detrimental when the model is continuously updated. Based on this analysis, in our work, we propose to freeze the text based classifiers and only modify the image representations through LayerNorm affine parameters, so that the model can be updated continuously without any reset.

### 2.3 Problem Statement

In open world single image test time adaptation, the model encounters individual test samples  $x_t$ , one at a time, originating from a test distribution  $\mathcal{D}_t$ . We explore the challenging scenario, where two types of out-of-distribution (OOD) samples are encountered during test time: (i) Weak OOD data denoted as  $\mathcal{D}_w$ , which have domain shift and label space  $\mathcal{Y} = \{1, \dots, C\}$ , where  $C$  denotes the number of known classes, which is of our interest; (ii) Strong OOD data  $\mathcal{D}_s$ , which have semantic shift (classes not of interest), i.e.,  $y_t \notin \mathcal{Y}$  for  $x_t \in \mathcal{D}_s$ . Here, as the test data can encompass both weak and strong OOD instances,  $\mathcal{D}_t = \mathcal{D}_w \cup \mathcal{D}_s$ . The goal is to first detect whether a test sample  $x_t$  arriving at time  $t$ , is a weak or strong OOD sample, which constitutes a binary classification task. Based on this, the model is adapted and then used for prediction. If  $x_t$  is identified as a weak OOD sample, a subsequent  $C$  class classification is performed, else the prediction is "I don't know". In essence, the overall process can be seen as a  $C + 1$  way classification problem. We also show that the method works without any modification for the *more challenging open world CTTA setting* as well, where the test domains can dynamically change with time.

To adapt the baseline prompt tuning methods [25, 26] for this setting, we update the prompts using their test time objective only if  $x_t$  is identified as a weak OOD sample. The test samples recognized as strong OOD are not used to update the prompts as they can adversely affect the model. We now describe the proposed ROSITA framework.

## 3 Proposed ROSITA Framework

In an open-world, a deployed model may encounter instances from unknown classes, which is not of interest. Such a scenario necessitates an OOD classifier to distinguish the unknown class samples from the known ones, which may otherwise adversely affect the model adaptation. Towards this goal, we utilize an effective LDA based parameter free OOD classifier [28, 22]. Subsequently, the model is adapted during test time, conditioned on the output of the OOD classifier.

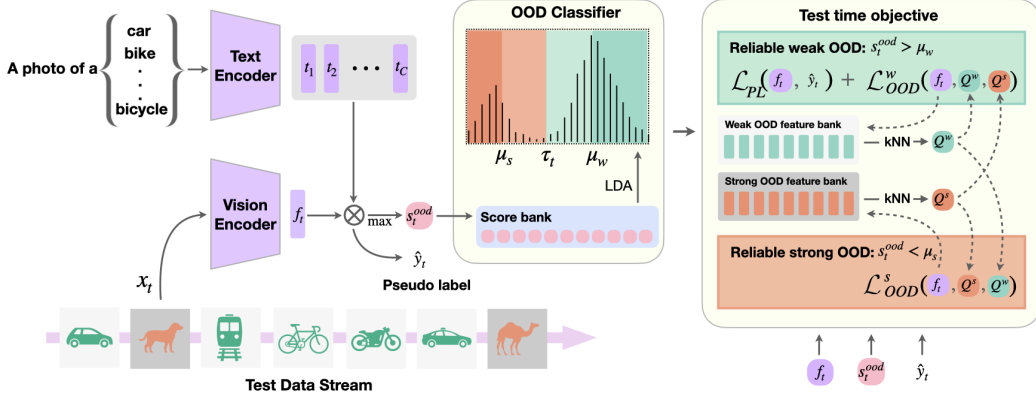


Figure 2: **ROSITA framework**: The test samples with **Weak** and **Strong** OOD data arrive one at a time. The image features are matched with the text based classifier, the confidence scores of which are used to distinguish between weak and strong OOD samples through a simple LDA based OOD classifier. Based on this classification and if a sample is identified to be reliable, the respective feature banks are updated and the proposed test-time objective is optimized to update the LayerNorm parameters of the Vision Encoder.

### 3.1 OOD Classifier

Contrary to closed world TTA setting, updating the model using all the test samples is not desirable in the open world scenario, where test samples can come from unknown classes. It is hence imperative to equip the model with the ability to say "I don't know" by rejecting the strong OOD samples from adapting the model. Here, we define the OOD score ( $s_t^{ood}$ ) of the test sample to be the maximum cosine similarity with the text embeddings as given below:

$$s_t^{ood} = \max_k \text{sim}(f_t, t_k); \quad k \in \{1, \dots, C\} \quad (1)$$

This problem can be viewed as a binary classification problem between weak and strong OOD samples based on the OOD score. Defining a threshold to discriminate between the two can be particularly challenging in the TTA scenario as the samples are only accessible in an online manner. To circumvent this issue, inspired by [22], we store the OOD scores of the test samples in a score bank  $\mathcal{S}$ , which is continuously updated in an online manner to store the latest  $|\mathcal{S}|$  scores, approximating the latest distribution of OOD scores of the test data. Given this, the optimal threshold can be estimated by performing 1D Linear Discriminant Analysis [28]. A simple linear search over a range of thresholds is done to identify the best threshold that minimizes the intra-class variance. For a threshold  $\tau$ , let  $\mathcal{S}_w = \{s_i | s_i > \tau, s_i \in \mathcal{S}\}$  and  $\mathcal{S}_s = \{s_i | s_i < \tau, s_i \in \mathcal{S}\}$  denote the set of scores identified as weak and strong OOD samples respectively. The optimal threshold  $\tau_t^*$  at time  $t$  is identified as the one that minimizes the intra class variance as follows

$$\tau_t^* = \arg \min_{\tau} \frac{1}{|\mathcal{S}_w|} \sum_{s \in \mathcal{S}_w} (s - \mu_w)^2 + \frac{1}{|\mathcal{S}_s|} \sum_{s \in \mathcal{S}_s} (s - \mu_s)^2 \quad (2)$$

where  $\mu_w$  and  $\mu_s$  are the means estimated from  $\mathcal{S}_w$  and  $\mathcal{S}_s$  respectively. The test sample  $x_t$  is classified as

$$\hat{y}_{OOD} = \begin{cases} 1 \text{ (weak OOD)} & \text{if } s_t^{ood} \geq \tau_t^* \\ 0 \text{ (strong OOD)} & \text{if } s_t^{ood} < \tau_t^* \end{cases} \quad (3)$$

The identified threshold  $\tau_t^*$  is used to reject the sample as strong OOD when  $s_t^{ood} < \tau_t^*$ . On the other hand, if it is detected to be a weak OOD sample with  $s_t^{ood} \geq \tau_t^*$ , we employ the TTA algorithm on the sample to update the model. *We equip all the baselines (Section 2.1) with this OOD classifier for fair comparison.* In Section B.4, we demonstrate the effectiveness of this LDA based OOD classifier in comparison with simple confidence thresholding with ROSITA. We now describe the TTA algorithm of ROSITA, also described in the Figure 2.

Table 1: Open world Test Time Adaptation results with CIFAR-10C and CIFAR-100C as weak OOD and four strong OOD datasets (MNIST, SVHN, Tiny-ImageNet, CIFAR-100C/10-C respectively). All methods use the same OOD detector described in Section 3.1. AUC, FPR and HM refer to the metrics AUROC, FPR95,  $Acc_{HM}$  respectively, defined in Section 3.2.

	Method	MNIST			SVHN			Tiny-ImageNet			CIFAR-100C/10-C			
		AUC $\uparrow$	FPR $\downarrow$	HM $\uparrow$	AUC $\uparrow$	FPR $\downarrow$	HM $\uparrow$	AUC $\uparrow$	FPR $\downarrow$	HM $\uparrow$	AUC $\uparrow$	FPR $\downarrow$	HM $\uparrow$	
CIFAR-10C	CLIP	ZS-Eval	91.91	85.04	75.57	89.93	64.20	74.08	91.33	27.07	74.63	82.57	67.92	68.89
		TPT	91.89	85.55	75.81	89.93	64.41	74.36	91.31	27.23	75.17	82.57	68.06	69.17
		TPT-C	81.64	67.53	74.86	58.48	71.72	48.26	74.08	61.45	49.88	61.45	94.30	46.10
	ROSITA	<b>99.10</b>	<b>7.63</b>	<b>84.17</b>	<b>94.79</b>	<b>32.59</b>	<b>78.80</b>	<b>96.43</b>	<b>12.10</b>	<b>80.06</b>	<b>82.99</b>	<b>62.89</b>	<b>69.56</b>	
	MAPLE	ZS-Eval	98.48	3.77	83.63	98.34	<b>7.86</b>	83.57	90.86	27.54	76.04	86.14	52.08	71.76
		TPT	98.15	5.67	81.56	98.34	7.89	82.73	90.86	27.61	75.46	86.15	52.14	70.94
		TPT-C	98.56	<b>3.74</b>	83.51	98.32	8.18	83.47	91.18	26.93	76.31	86.50	50.56	71.07
	PAAlign	98.15	5.67	82.24	<b>98.34</b>	7.90	83.51	90.86	27.60	75.98	86.15	52.18	71.52	
	PAlign-C	98.56	3.74	83.49	98.32	8.13	83.46	91.18	26.90	76.30	86.50	50.58	71.04	
	ROSITA	<b>99.34</b>	5.22	<b>87.63</b>	97.80	13.15	<b>84.17</b>	<b>91.67</b>	<b>25.31</b>	<b>77.67</b>	<b>86.82</b>	<b>50.33</b>	<b>73.15</b>	
CIFAR-100C	CLIP	ZS-Eval	77.78	99.93	48.39	64.70	98.68	45.85	67.31	73.89	45.80	63.28	93.25	44.04
		TPT	77.76	99.94	48.33	64.71	98.63	45.85	67.28	73.82	45.93	63.26	93.20	44.02
		TPT-C	51.57	100.00	27.04	9.40	99.98	5.74	59.74	79.76	18.41	55.86	<b>86.35</b>	13.64
	ROSITA	<b>96.07</b>	<b>19.28</b>	<b>57.34</b>	<b>82.09</b>	<b>64.64</b>	<b>48.17</b>	<b>83.55</b>	<b>50.76</b>	<b>55.88</b>	<b>68.54</b>	89.71	<b>47.98</b>	
	MAPLE	ZS-Eval	87.43	64.19	54.97	92.98	40.51	56.42	68.80	74.35	48.24	66.93	87.94	46.06
		TPT	87.42	64.09	53.09	92.97	40.44	54.37	68.80	<b>74.20</b>	46.97	66.93	87.95	44.38
		TPT-C	87.65	63.08	55.14	93.09	40.30	56.31	68.85	74.71	48.53	66.97	87.94	46.30
	PAAlign	87.42	64.11	53.98	92.97	40.48	55.37	68.80	74.23	47.69	66.93	87.93	45.16	
	PAlign-C	88.25	57.31	55.69	93.45	39.39	57.39	68.76	78.12	48.15	66.82	87.80	47.01	
	ROSITA	<b>97.04</b>	<b>11.01</b>	<b>62.06</b>	<b>96.26</b>	<b>20.99</b>	<b>59.25</b>	<b>70.37</b>	77.00	<b>48.68</b>	<b>69.57</b>	<b>83.61</b>	<b>48.80</b>	

### 3.2 Test Time Adaptation

Given a single test sample  $x_t$  at time  $t$ , it is first characterized into a weak or strong OOD sample using the OOD classifier described above. This is important, since, using strong OOD samples for model adaptation can have a negative impact on the model. In this work, we propose a test time objective that can leverage both the weak and strong OOD samples through a feature bank to enhance the discriminability between them.

We first identify a test sample  $x_t$  as a reliable weak or strong OOD sample based on the OOD score. As we have access to an approximate distribution of the OOD scores as described in the OOD classifier, we leverage the statistics of weak and strong OOD samples estimated through LDA to identify reliable samples. A test sample  $x_t$  is said to be a reliable weak OOD sample if its OOD score  $s_t^{ood} > \mu_w$  and a reliable strong OOD sample if its OOD score  $s_t^{ood} < \mu_s$ . We leverage these reliable test samples to increase the separability between weak and strong OOD samples through a contrastive objective. A contrastive objective typically needs positives and negatives, the goal being to maximize the similarity between a sample and its positive (could be augmentation [32] or nearest neighbours [33]), while minimizing its similarity with the negatives. Such objectives [32] [34, 35, 33] have been extensively used to learn good image representations in a self-supervised way. While self-supervised learning assumes access to abundant data in an offline manner giving the freedom to carefully choose positives and negatives, this problem is set in an online scenario, where the test samples arrive one at a time and are accessible only at that instant. This challenging setting makes it non trivial to use objectives like [33]. To circumvent this issue of lack of abundant test data, we propose to store two dynamically updated feature banks  $\mathcal{M}_w$  and  $\mathcal{M}_s$  of sizes  $N_w$  and  $N_s$ , to store the identified reliable weak and strong OOD sample features respectively. We propose an OOD discriminative objective to contrast the reliable samples by choosing its positives and negatives as the  $K$  nearest neighbours from the feature banks  $\mathcal{M}_w$  and  $\mathcal{M}_s$  respectively. The buffer size for  $\mathcal{M}_w$  is set as  $N_w = C \times K$ , where  $C$  is the number of known classes and  $K$  is the number of neighbours retrieved. The feature bank  $\mathcal{M}_w$  or  $\mathcal{M}_s$  is updated with the test sample feature  $f_t$  if it is detected as a reliable weak or strong OOD sample respectively.

We fetch the  $K$  nearest neighbours of a reliable test sample  $x_t$  from each feature bank as follows.

$$Q_w = \text{kNN}(f_t; \mathcal{M}_w); \quad Q_s = \text{kNN}(f_t; \mathcal{M}_s) \quad (4)$$

Table 2: Results with ImageNet-C/R as weak OOD, MNIST and SVHN as strong OOD datasets.

Method	IN-C/MNIST			IN-C/SVHN			IN-R/MNIST			IN-R/SVHN			
	AUC $\uparrow$	FPR $\downarrow$	HM $\uparrow$	AUC $\uparrow$	FPR $\downarrow$	HM $\uparrow$	AUC $\uparrow$	FPR $\downarrow$	HM $\uparrow$	AUC $\uparrow$	FPR $\downarrow$	HM $\uparrow$	
CLIP	ZS-Eval	93.39	55.52	41.43	85.89	72.91	40.83	91.27	91.09	71.50	90.43	75.04	71.66
	TPT	93.12	58.01	42.21	85.43	74.47	40.95	91.25	91.23	71.98	90.43	74.98	72.36
	TPT-C	56.57	99.12	6.19	11.38	100.00	7.24	82.81	85.79	68.25	80.94	80.03	69.18
	ROSITA	<b>99.52</b>	<b>4.06</b>	<b>48.53</b>	<b>98.34</b>	<b>10.21</b>	<b>46.32</b>	<b>99.44</b>	<b>4.29</b>	<b>83.53</b>	<b>98.62</b>	<b>9.08</b>	<b>80.75</b>
MAPLE	ZS-Eval	81.49	92.95	41.70	83.26	71.15	42.77	90.15	83.54	74.42	92.74	65.70	75.71
	TPT	81.38	93.17	39.92	83.18	71.52	40.93	90.14	83.58	74.00	92.74	65.68	75.23
	TPT-C	83.25	87.60	42.81	83.18	70.60	42.86	90.35	81.49	74.73	92.79	65.20	75.59
	PAlign	81.38	93.17	41.32	83.18	71.52	42.30	90.14	83.58	74.66	92.74	65.68	75.93
	PAlign-C	71.22	86.32	27.14	32.17	94.32	15.44	92.20	59.70	75.23	93.54	54.59	75.67
	ROSITA	<b>99.56</b>	<b>1.66</b>	<b>51.30</b>	<b>98.68</b>	<b>5.09</b>	<b>50.67</b>	<b>99.39</b>	<b>2.95</b>	<b>84.70</b>	<b>97.85</b>	<b>12.98</b>	<b>83.07</b>

**Case 1: Reliable weak OOD sample.** If a test sample is identified as a reliable weak OOD sample, we use a pseudo label loss on the sample  $x_t$  and its augmentation  $\tilde{x}_t$  as follows:

$$\mathcal{L}_{PL} = \mathcal{L}_{CE}(x_t, \hat{y}_t) + \mathcal{L}_{CE}(\tilde{x}_t, \hat{y}_t); \quad \hat{y}_t = \operatorname{argmax}_i \operatorname{sim}(f_t, t_i) \quad (5)$$

Further, we also propose to use a contrastive objective to enhance the clustering of weak OOD samples while pushing them apart from the strong OOD samples. As we aim to correctly classify the weak OOD samples, we select positives  $z^+$  from  $Q_w$  if its prediction  $y^+$  matches with that of the sample  $\hat{y}_t$ . The features  $Q_s$  constituting of its kNN from the strong OOD feature bank  $M_s$  act as the negatives. The following is the weak OOD contrastive objective:

$$\mathcal{L}_{OOD}^w = -\frac{1}{K^+} \sum_{z^+ \in Q_w} \mathbb{1}(y^+ = \hat{y}_t) \log \frac{\exp(\operatorname{sim}(f_t, z^+)/\tau)}{\sum_{z^- \in Q_s} \exp(\operatorname{sim}(f_t, z^-)/\tau)} \quad (6)$$

where  $K^+ = \sum_{z^+ \in Q_w} \mathbb{1}(y^+ = \hat{y}_t)$ , is the number of neighbours positively matched with  $\hat{y}_t$ .

**Case 2: Reliable strong OOD sample.** If a test sample is identified as a reliable strong OOD sample, we use the following contrastive objective to increase the separability of weak and strong OOD samples by selecting positives  $z^+$  from  $Q_s$  and negatives  $z^-$  from  $Q_w$ :

$$\mathcal{L}_{OOD}^s = -\frac{1}{K} \sum_{z^+ \in Q_s} \log \frac{\exp(\operatorname{sim}(f_t, z^+)/\tau)}{\sum_{z^- \in Q_w} \exp(\operatorname{sim}(f_t, z^-)/\tau)} \quad (7)$$

The LayerNorm parameters of the Vision Encoder are updated to minimize the following test time objective to adapt the model one sample at a time in an online manner:

$$\mathcal{L}_{TTA} = \begin{cases} \mathcal{L}_{PL} + \mathcal{L}_{OOD}^w & \text{if } \hat{y}_{OOD} = 1; s_t^{ood} > \mu_w \\ \mathcal{L}_{OOD}^s & \text{if } \hat{y}_{OOD} = 0; s_t^{ood} < \mu_s \end{cases} \quad (8)$$

This objective improves the proximity between the test sample and its positives, suitably chosen based on its OOD prediction  $\hat{y}_{OOD}$ , while also pushing apart the test sample and its negatives. This collectively encourages the model to adapt such that weak OOD samples are clustered and farther apart from strong OOD samples, improving the OOD detection and classification performance.

**Evaluation Metrics.** We employ standard metrics, namely AUROC (Area Under the Receiver Operating Characteristic Curve) and FPR95 (False Positive Rate at a True Positive Rate of 95%), from the OOD detection literature [23, 22, 27]. Additionally, we compute the classification accuracy for weak OOD samples ( $Acc_W$ ) and the binary classification accuracy for correctly recognizing strong OOD samples ( $Acc_S$ ) as defined below. To gauge the overall performance, we compute  $Acc_{HM}$  (HM), representing the harmonic mean of  $Acc_W$  and  $Acc_S$ , which serves as a comprehensive metric capturing the trade-off between  $Acc_W$  and  $Acc_S$ . Here, we summarily report AUROC (AUC), FPR95 (FPR) and  $Acc_{HM}$  (HM) for all the datasets (All five metrics are reported in detail in Appendix D).

$$Acc_W = \frac{\sum_{(x_i, y_i) \in \mathcal{D}_t} \mathbb{1}(y_i = \hat{y}_i) \cdot \mathbb{1}(y_i \in \mathcal{Y})}{\sum_{x_i, y_i \in \mathcal{D}_t} \mathbb{1}(y_i \in \mathcal{Y})}; \quad Acc_S = \frac{\sum_{(x_i, y_i) \in \mathcal{D}_t} \mathbb{1}(\hat{y}_i, OOD = 0) \cdot \mathbb{1}(y_i \notin \mathcal{Y})}{\sum_{x_i, y_i \in \mathcal{D}_t} \mathbb{1}(y_i \notin \mathcal{Y})} \quad (9)$$

## 4 Experiments

**Datasets.** We experiment with a diverse set of datasets for weak and strong OOD data. For weak OOD, we use CIFAR-10C [5], CIFAR-100C [5], ImageNet-C [5] from the corruption category and ImageNet-R [36], VisDA [37] as style transfer datasets. We use MNIST [38], SVHN [39], CIFAR-10/100C [5] and TinyImageNet [40] datasets for strong OOD data. We describe the datasets in detail in the Appendix A.3.1.

**Implementation Details.** We use CLIP and MaPLe VLMs with ViT-B16 architecture. We use SGD optimizer with a learning rate of 0.001 to update the LayerNorm parameters of the Vision encoder. We set the size of OOD score bank  $S$  to 512, number of neighbours  $K$  to 5 and the strong OOD feature bank size  $N_s$  to 64. For TPT and PAlign, we use the same hyperparameters given in their papers [25, 26]. For TPT-C and PAlign-C, we use SGD with learning rate of  $10^{-5}$  on experimenting with different learning rates A.3.2. All experiments are done on a single NVIDIA A6000 GPU.

Table 3: Results with VisDA as weak OOD data.

Method	VisDA/MNIST			VisDA/SVHN			
	AUC $\uparrow$	FPR $\downarrow$	HM $\uparrow$	AUC $\uparrow$	FPR $\downarrow$	HM $\uparrow$	
CLIP	ZS-Eval	93.55	65.88	78.28	90.46	65.03	77.03
	TPT	93.56	66.04	78.42	90.47	65.05	77.24
	TPT-C	81.84	86.12	75.35	81.24	91.32	70.35
	ROSITA	<b>99.59</b>	<b>3.26</b>	<b>90.64</b>	<b>98.89</b>	<b>6.48</b>	<b>89.12</b>
MaPLe	ZS-Eval	93.07	66.00	80.24	94.41	40.56	80.21
	TPT	93.07	66.11	80.31	94.41	40.51	80.28
	TPT-C	95.67	27.45	82.05	94.53	38.87	80.28
	PAlign	93.07	66.11	80.63	94.41	40.51	80.61
	PAlign-C	95.60	27.97	81.92	95.67	26.87	82.06
	ROSITA	<b>99.80</b>	<b>1.41</b>	<b>90.83</b>	<b>98.87</b>	<b>6.48</b>	<b>89.68</b>

## 5 Analysis

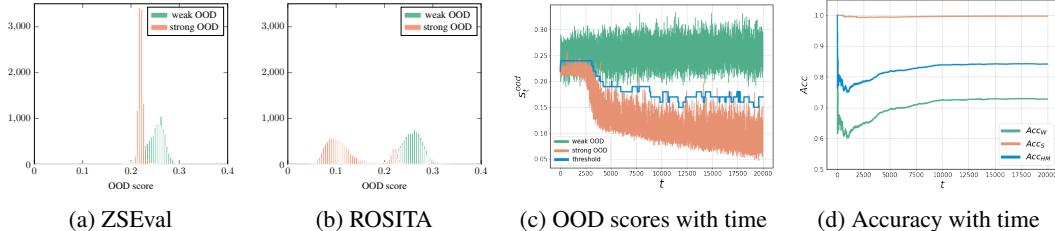


Figure 3: Histograms of OOD scores for ZS-Eval (a) and ROSITA (b) on CIFAR-10C/MNIST dataset. (c) Change in OOD scores of **Weak** and **Strong** OOD samples, the best threshold with time  $t$ ; (d) Accuracy metrics measured for samples seen until time  $t$ . Using the LDA based OOD classifier with ROSITA, the weak and strong OOD samples separate better and the accuracy metrics improve with time. *Analysis on OOD classifier and parameter  $K$  is presented in Appendix B.4 and B.2.*

**Comparison with prior methods.** We observe, from Table 1, 2, 3 that TPT and PAlign perform similar to ZSEval in most datasets, as the prompts are reset after every single image update. On continuously updating prompts in TPT-C and PAlign-C, we observe the HM to reduce compared to ZS-Eval. The effect is more severe with CLIP when compared to MaPLe, as only the text prompts are updated keeping the vision encoder fixed (as also observed in Section 2.2). ROSITA, being equipped with a carefully designed objective to better discriminate between weak and strong OOD samples (Figure 3), results in overall better metrics in general. We report *additional experimental results using CLIP with ViT-B/32 and ResNet-50 architecture in C.3 and with different corruption types in C.2.*

**Loss Ablation.** We perform experiments to study the importance of each loss component. The first row in Table 4 refers to ZS-Eval results. We observe that only using  $\mathcal{L}_{PL}$  or  $\mathcal{L}_{OOD}^w$  improves the metrics for CIFAR-10C dataset. For ImageNet-R (IN-R) as weak OOD data, using  $\mathcal{L}_{PL}$  or  $\mathcal{L}_{OOD}^w$  is observed to increase FPR and decrease HM. IN-R has 200 classes and hence is a more confusing classification task compared to CIFAR-10C. This decrease in performance for IN-R can be attributed to the misclassification of some strong OOD samples as reliable weak OOD, increasing the confusion between weak and strong OOD samples. Using  $\mathcal{L}_{OOD}^s$  significantly

Table 4: Ablation study on loss components.

$\mathcal{L}_{PL}$	$\mathcal{L}_{OOD}^w$	$\mathcal{L}_{OOD}^s$	CIFAR-10C/MNIST			IN-R/MNIST		
			AUC $\uparrow$	FPR $\downarrow$	HM $\uparrow$	AUC $\uparrow$	FPR $\downarrow$	HM $\uparrow$
$\times$	$\times$	$\times$	91.91	85.04	75.57	91.27	91.09	71.5
$\checkmark$	$\times$	$\times$	95.29	30.82	80.97	81.07	99.02	64.32
$\times$	$\checkmark$	$\times$	95.23	28.91	79.71	87.73	94.67	67.28
$\times$	$\times$	$\checkmark$	98.61	12.73	79.84	99.39	4.81	80.82
$\times$	$\checkmark$	$\checkmark$	99.27	<b>4.15</b>	80.69	99.48	4.40	81.92
$\checkmark$	$\checkmark$	$\checkmark$	<b>99.10</b>	7.63	<b>84.17</b>	<b>99.44</b>	<b>4.29</b>	<b>83.53</b>



reduces the confusion between weak and strong OOD samples, shown by the significant drop in FPR compared to ZSEval. The contrastive objective to separate the OOD samples, in conjunction with  $\mathcal{L}_{PL}$  which aids to improve the weak OOD classification, gives the overall best results. We further *analyse the OOD score histograms, which we present in Appendix B.3* supporting our observations.

**Open World Continuous Test Time Adaptation.** We perform experiments by sequentially presenting 15 corruptions from CIFAR-10C along with strong OOD samples from MNIST. To the best of our knowledge, we are the first to explore this challenging open world scenario in CTTA. From Table 5 (and *additional results in Appendix C.4*), we observe that ROSITA consistently outperforms prior methods even in this scenario of long term and continuously changing domains.

Table 5:  $Acc_{HM}$  on Openworld CTTA for CIFAR-10C/MNIST (15 corruptions shown sequentially)

Method	<i>gaussian</i>	<i>shot</i>	<i>impulse</i>	<i>defocus</i>	<i>glass</i>	<i>motion</i>	<i>zoom</i>	<i>snow</i>	<i>frost</i>	<i>fog</i>	<i>brightness</i>	<i>contrast</i>	<i>elastic</i>	<i>pixelate</i>	<i>jpeg</i>	Mean	
CLIP	ZS-Eval	43.21	47.74	<b>57.68</b>	75.43	38.56	73.91	76.94	75.56	79.38	74.36	84.88	67.36	55.61	60.56	53.82	64.33
	TPT	43.15	47.66	57.70	75.36	38.22	73.70	76.84	75.49	79.32	74.80	84.82	67.46	55.50	60.40	53.48	64.26
	TPT-C	30.06	25.92	31.05	52.71	20.88	45.97	53.08	21.61	26.83	38.80	38.88	37.40	33.83	35.26	3.53	33.05
	ROSITA	<b>43.35</b>	<b>48.21</b>	57.04	<b>78.01</b>	<b>43.29</b>	<b>77.48</b>	<b>80.16</b>	<b>76.84</b>	<b>80.15</b>	<b>76.26</b>	<b>86.33</b>	<b>73.44</b>	<b>60.35</b>	<b>61.55</b>	<b>60.38</b>	<b>66.86</b>

**Varying OOD ratio.** We simulate various practical scenarios using CIFAR-10C/MNIST dataset by varying the ratio of weak to strong OOD samples in the test stream as 0.2, 0.4, 0.6, 0.8. Table 6 shows that ROSITA performs better than all baselines across all ratios, reinforcing the robustness of the proposed method. We perform further *experiments on ImageNet-R and MaPLE backbone as well, which we report in Appendix C.1*.

Table 6:  $Acc_{HM}$  on varying OOD ratio.

Ratio	0.2	0.3	0.6	0.8	
CLIP	ZS-Eval	75.56	75.59	75.57	75.56
	TPT	75.67	75.75	75.81	75.83
	TPT-C	72.70	74.31	74.79	75.16
	ROSITA	<b>82.96</b>	<b>83.97</b>	<b>84.51</b>	<b>84.37</b>

**Complexity Analysis** For prompt tuning methods TPT-C and PAlign-C, the GPU memory and time taken(secs/image) scales with the number of classes, as it requires more memory to store the intermediate activations and gradients. The time taken to perform forward and backward pass through the text encoder also depends on the number of classes. On the other hand, ROSITA requires two forward passes and one backward pass through the vision encoder for reliable test samples. For e.g., for ImageNet-C dataset with 1000 classes, ZSEval, TPT and ROSITA require 5.71 GB, 23.24 GB and 5.73 GB GPU memory to perform a single image based model update. Hence, ROSITA is computationally very efficient (of the order of ZSEval, from Figure 4).

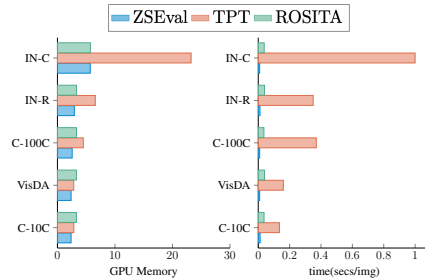


Figure 4: Complexity Analysis of different methods using CLIP backbone. *This analysis for MaPLE is in Appendix B.5.*

## 6 Conclusion

In this work, we propose ROSITA, a novel framework to address the challenging problem of Open-world Test Time Adaptation (TTA) on a single image basis. Our proposed method effectively distinguishes between weak and strong Out of Distribution (OOD) samples by leveraging dynamically updated feature banks. It facilitates effective model adaptation by using reliable test samples, while mitigating the negative impact of undesirable samples. Through extensive experimentation on diverse domain adaptation benchmarks, we have demonstrated the effectiveness of ROSITA in several scenarios inspired by the dynamic real world environment.

**Limitations** The proposed method while being simple and efficient, leverages a feature bank, which could be a constraint in certain applications. While ROSITA performs better than the baselines, in datasets like weak/strong OOD being CIFAR-10/100C, the FPR indicates that there is still significant scope for improvement.

## References

- [1] J. Deng, W. Dong, R. Socher, L. J. Li, K. Li, and L. Fei-Fei. “ImageNet: A large-scale hierarchical image database”. In: *CVPR*. 2009.
- [2] S. Ren, K. He, R. Girshick, and J. Sun. “Faster R-CNN: Towards Real-Time Object Detection with Region Proposal Networks”. In: *NeurIPS*. 2015.
- [3] K. He, G. Gkioxari, P. Dollár, and R. Girshick. “Mask R-CNN”. In: *ICCV*. 2017.
- [4] M. Everingham, L. Gool, C. K. Williams, J. Winn, and A. Zisserman. “The Pascal Visual Object Classes (VOC) Challenge”. In: *IJCV* (2010).
- [5] D. Hendrycks and T. Dietterich. “Benchmarking neural network robustness to common corruptions and perturbations”. In: *arXiv preprint arXiv:1903.12261* (2019).
- [6] X. Peng, Q. Bai, X. Xia, Z. Huang, K. Saenko, and B. Wang. “Moment matching for multi-source domain adaptation”. In: *ICCV*. 2019.
- [7] Y. Ganin, E. Ustinova, H. Ajakan, P. Germain, H. Larochelle, F. Laviolette, M. Marchand, and V. Lempitsky. “Domain-adversarial training of neural networks”. In: *JMLR* (2016).
- [8] K. Saito, K. Watanabe, Y. Ushiku, and T. Harada. “Maximum classifier discrepancy for unsupervised domain adaptation”. In: *CVPR*. 2018.
- [9] Y. Jin, X. Wang, M. Long, and J. Wang. “Minimum class confusion for versatile domain adaptation”. In: *ECCV*. 2020.
- [10] J. Liang, D. Hu, and J. Feng. “Do We Really Need to Access the Source Data? Source Hypothesis Transfer for Unsupervised Domain Adaptation”. In: *ICML*. 2020.
- [11] S. Yang, J. van de Weijer, L. Herranz, S. Jui, et al. “Exploiting the intrinsic neighborhood structure for source-free domain adaptation”. In: *NeurIPS*. 2021.
- [12] S. Yang, Y. Wang, K. Wang, S. Jui, et al. “Attracting and dispersing: A simple approach for source-free domain adaptation”. In: *NeurIPS*. 2022.
- [13] N. Karim, N. C. Mithun, A. Rajvanshi, H.-p. Chiu, S. Samarasekera, and N. Rahnavard. “C-SFDA: A Curriculum Learning Aided Self-Training Framework for Efficient Source Free Domain Adaptation”. In: *CVPR*. 2023.
- [14] D. Wang, E. Shelhamer, S. Liu, B. Olshausen, and T. Darrell. “Tent: Fully Test-Time Adaptation by Entropy Minimization”. In: *ICLR*. 2021.
- [15] S. Schneider, E. Rusak, L. Eck, O. Bringmann, W. Brendel, and M. Bethge. “Improving robustness against common corruptions by covariate shift adaptation”. In: *NeurIPS*. 2020.
- [16] S. Niu, J. Wu, Y. Zhang, Y. Chen, S. Zheng, P. Zhao, and M. Tan. “Efficient test-time model adaptation without forgetting”. In: *ICML*. 2022.
- [17] D. Chen, D. Wang, T. Darrell, and S. Ebrahimi. “Contrastive test-time adaptation”. In: *CVPR*. 2022.
- [18] R. A. Marsden, M. Döbler, and B. Yang. “Universal Test-time Adaptation through Weight Ensembling, Diversity Weighting, and Prior Correction”. In: *WACV*. 2024.
- [19] Q. Wang, O. Fink, L. Van Gool, and D. Dai. “Continual Test-Time Domain Adaptation”. In: *CVPR*. 2022.
- [20] M. Döbler, R. A. Marsden, and B. Yang. “Robust mean teacher for continual and gradual test-time adaptation”. In: *CVPR*. 2023.
- [21] G. Chakrabarty, M. Sreenivas, and S. Biswas. “SANTA: Source Anchoring Network and Target Alignment for Continual Test Time Adaptation”. In: *Transactions on Machine Learning Research* (2023).
- [22] Y. Li, X. Xu, Y. Su, and K. Jia. “On the robustness of open-world test-time training: Self-training with dynamic prototype expansion”. In: *ICCV*. 2023.
- [23] J. Lee, D. Das, J. Choo, and S. Choi. “Towards open-set test-time adaptation utilizing the wisdom of crowds in entropy minimization”. In: *ICCV*. 2023.
- [24] A. Radford, J. W. Kim, C. Hallacy, A. Ramesh, G. Goh, S. Agarwal, G. Sastry, A. Askell, P. Mishkin, J. Clark, et al. “Learning transferable visual models from natural language supervision”. In: *ICML*. PMLR. 2021.
- [25] M. Shu, W. Nie, D.-A. Huang, Z. Yu, T. Goldstein, A. Anandkumar, and C. Xiao. “Test-time prompt tuning for zero-shot generalization in vision-language models”. In: *NeurIPS*. 2022.

- [26] J. H. A. Samadh, H. Gani, N. H. Hussein, M. U. Khattak, M. Naseer, F. Khan, and S. Khan. “Align your prompts: Test-time prompting with distribution alignment for zero-shot generalization”. In: *NeurIPS*. 2023.
- [27] H. Wang, Y. Li, H. Yao, and X. Li. “Clipn for zero-shot ood detection: Teaching clip to say no”. In: *ICCV*. 2023.
- [28] R. A. Fisher. “The use of multiple measurements in taxonomic problems”. In: *Annals of eugenics* 7.2 (1936), pp. 179–188.
- [29] M. U. Khattak, H. Rasheed, M. Maaz, S. Khan, and F. S. Khan. “Maple: Multi-modal prompt learning”. In: *CVPR*. 2023.
- [30] B. Zhao, H. Tu, C. Wei, J. Mei, and C. Xie. “Tuning LayerNorm in Attention: Towards efficient multi-modal llm finetuning”. In: *arXiv preprint arXiv:2312.11420* (2023).
- [31] M. Sreenivas, G. Chakrabarty, and S. Biswas. “pSTarC: Pseudo Source Guided Target Clustering for Fully Test-Time Adaptation”. In: *WACV*. 2024.
- [32] T. Chen, S. Kornblith, M. Norouzi, and G. Hinton. “A simple framework for contrastive learning of visual representations”. In: *ICML*. 2020.
- [33] D. Dwibedi, Y. Aytar, J. Tompson, P. Sermanet, and A. Zisserman. “With a little help from my friends: Nearest-neighbor contrastive learning of visual representations”. In: *ICCV*. 2021.
- [34] K. He, H. Fan, Y. Wu, S. Xie, and R. Girshick. “Momentum contrast for unsupervised visual representation learning”. In: *CVPR*. 2020.
- [35] P. Khosla, P. Teterwak, C. Wang, A. Sarna, Y. Tian, P. Isola, A. Maschinot, C. Liu, and D. Krishnan. “Supervised contrastive learning”. In: *NeurIPS*. 2020.
- [36] D. Hendrycks, S. Basart, N. Mu, S. Kadavath, F. Wang, E. Dorundo, R. Desai, T. Zhu, S. Parajuli, M. Guo, et al. “The many faces of robustness: A critical analysis of out-of-distribution generalization”. In: *CVPR*. 2021.
- [37] X. Peng, B. Usman, N. Kaushik, J. Hoffman, D. Wang, and K. Saenko. “Visda: The visual domain adaptation challenge”. In: *arXiv preprint arXiv:1710.06924* (2017).
- [38] Y. LeCun, L. Bottou, Y. Bengio, and P. Haffner. “Gradient-based learning applied to document recognition”. In: *Proceedings of the IEEE* 86.11 (1998), pp. 2278–2324.
- [39] Y. Netzer, T. Wang, A. Coates, A. Bissacco, B. Wu, A. Y. Ng, et al. “Reading digits in natural images with unsupervised feature learning”. In: *NIPS workshop on deep learning and unsupervised feature learning*. Vol. 2011. 5. Granada, Spain. 2011, p. 7.
- [40] Y. Le and X. Yang. “Tiny imagenet visual recognition challenge”. In: *CS 231N 7.7* (2015), p. 3.

## A Appendix

### A.1 Broader Impact

We address the problem of open world single image test time adaptation of Vision Language Models. We believe these large scale pretrained VLMs capability of recognizing a wide variety of objects can be very useful for deploying in an open real world environment. However, it needs to be equipped with such capabilities to make informed decisions. In this work, specifically, we equip the "VLM" to say "I don't know" if the model encounters an object which is not of interest. The robustness and generalization of VLMs on encountering a variety of distribution shifts are extensively studied in this work. We believe this work can serve as a strong baseline to study open world adaptation capabilities of VLMs. Although the proposed method has been tested in several simulated real world scenarios, in order to deploy such a method in real world, more robust tests need to be done to prevent, say test time adversarial attacks etc.

### A.2 License information of the assets used in this work

**Datasets:** The following are the license information for the datasets used in this paper. Datasets under Apache License: CIFAR-10C [5], CIFAR-100C [5], ImageNet-C [5]. Datasets under MIT License: ImageNet-R [36]. Datasets under Creative Commons Attribution-Share Alike 3.0 License: MNIST [38]. The License information for datasets TinyImageNet [40], VisDA [37], SVHN [39] could not be found.

**Models:** We use CLIP [24] model provided by OpenAI through MIT License. MaPLe [29] model has no license associated with it.

**Code:** We adapt the existing TTA methods [25, 26] for this problem setting. The code for TPT [25] is released with MIT License. The code for PromptAlign [26] has no license associated with it.

### A.3 Implementation Details

#### A.3.1 Datasets

We experiment with a diverse set of datasets, encompassing corruption datasets, style transfer datasets, and other common datasets.

**CIFAR10-C** [5] is a small-scale corruption dataset of 10 classes with 15 common corruption types. It consists of 10,000 images for each corruption.

**CIFAR-100C** [5] is also a corruption dataset with 100 classes and 15 corruption types. It also consists of 10,000 images for each corruption.

**ImageNet-C** [5] is a large-scale corruption dataset spanning 1000 categories with a total of 50,000 images. 15 types of corruption images are synthesized from these 50,000 images.

**ImageNet-R** [36] is a realistic style transfer dataset encompassing interpretations of 200 ImageNet classes, amounting to a total of 30,000 images.

**VisDA** [37] is a synthetic-to-real large-scale dataset, comprising of 152,397 synthetic training images and 55,388 real testing images across 12 categories.

**MNIST** [38] is a dataset of handwritten images consisting of 60,000 training and 10,000 testing images.

**SVHN** [39] is also a digits dataset with house numbers captured from real streets. It consists of 50,000 training images and 10,000 testing images.

We perform experiments on five weak OOD datasets. The corresponding strong OOD datasets are chosen such that there is no overlap between weak and strong OOD datasets and is described in Table 7. The 15 corruptions fall into four categories: synthetic weather effects, per-pixel noise, blurring, and digital transforms. *snow* corruption is a synthesized weather effect on which all the main experiments of CIFAR-10C, CIFAR-100C and ImageNet-C are done. To evaluate the robustness of our method across different corruption types, we do additional experiments with *impulse noise*

, *motion blur* and *jpeg compression* corruptions from the categories per-pixel noise, blurring and digital transforms respectively and report the results in Section C.2.

Table 7: Details of Weak and strong OOD dataset combinations

Datasets		# images		
Weak OOD	Strong OOD	weak	strong	total
CIFAR-10C	MNIST, SVHN, Tiny ImageNet, CIFAR-100C	10000	10000	20000
CIFAR-100C	MNIST, SVHN, Tiny ImageNet, CIFAR-10C	10000	10000	20000
ImageNet-C	MNIST, SVHN	50000	50000	100000
ImageNet-R	MNIST, SVHN	30000	30000	60000
VisDA	MNIST, SVHN	50000	50000	100000

### A.3.2 Methods

Here, we describe the parameters chosen for all the baseline methods and our proposed method.

**TPT [25]:** The prompt is initialized with the default "A photo of a" text. The corresponding 4 tokens in the input text embedding space are optimized for each test image. The prompt is **reset** after each update. A single test image is augmented 63 times using random resized crops to create a batch of 64 images. The confident samples with 10% lowest entropy are selected. The test time loss is the entropy of the averaged prediction of the selected confident samples. AdamW optimizer with a learning rate of  $5e^{-4}$  is used, following [25].

**PAlign [26]:** Following PromptAlign [26], MaPLe [29] model trained on ImageNet using 16-shot training data with 2 prompt tokens for a depth of 3 layers is used. The prompts on both the text and vision encoders are optimized on a single test image. Similar to TPT, 10% of 64 augmentations are selected to compute the entropy loss. The token distribution loss to align the token statistics of test with that of source data is computed for all 64 images. AdamW optimizer with a learning rate of  $5e^{-4}$  to update the prompts for each image, following [26]. The prompts are **reset** to the ImageNet trained prompts after each update.

**TPT-C / PAlign-C:** We create the continuous prompt update versions of TPT and PAlign as TPT-C and PAlign-C respectively. The only difference is that the prompts are continuously updated using the test stream of samples. If a sample is detected as reliable weak OOD, the respective test time objectives are used to update the prompts. For this purpose, we vary the learning rate and optimizer to select the best optimizer for continuous prompt update. On performing experiments on CIFAR-10C/MNIST data, from Figure 5 we observe that SGD optimizer with learning rate  $10^{-5}$  works the best for continuous prompt update and hence we use this for all the experiments of TPT-C and PAlign-C.

**ROSITA:** We use SGD optimizer with a learning rate of 0.001 to update the LayerNorm affine parameters of the Vision encoder. We set the size of OOD score bank  $\mathcal{S}$  to 512, number of neighbours  $K$  to 5 and the strong OOD feature bank size  $N_s$  to 64.

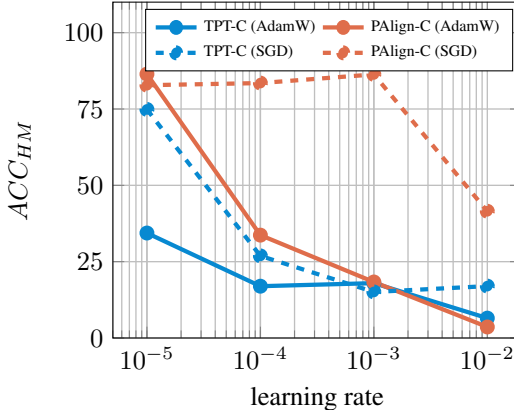


Figure 5: Performance of TPT-C and PAlign-C for CIFAR-10C/MNIST with AdamW and SGD optimizer on varying learning rates.

## B Additional Analysis

In this section, in addition to the analysis done in Section 5, we study the robustness of the proposed method ROSITA more extensively, in the terms of (1) Error bars on different test data streams, (2) Role of the parameter  $K$ , the number of neighbours, (3) Analysis of OOD scores on using different combinations of the proposed loss components, (4) Effectiveness of LDA based OOD detector in comparison with simple thresholding, (5) Complexity Analysis of MaPLe backbone.

### B.1 Analysis on error bars

To study the robustness of our method for differently ordered test streams, we run ROSITA with five random seeds and report the Mean and Standard deviation of the  $Acc_{HM}$  in Table 8 for CIFAR-10C/100C as weak OOD data and MNIST, SVHN, Tiny ImageNet, CIFAR-100C/10C as strong OOD data (corresponding to our results in Table 1 in the main paper). We observe that the variance in the performance of ROSITA is very low, reinforcing the robustness of the proposed method for different shuffled datasets and augmentations created.

Table 8: Performance (Mean and Standard deviation of  $Acc_{HM}$ ) of ROSITA across 5 random seeds for CIFAR-10/100C as weak OOD data with 4 strong OOD datasets.

Dataset	MNIST	SVHN	Tiny	CIFAR-100/10C
CIFAR-10C	$84.07 \pm 0.023$	$78.90 \pm 0.038$	$80.10 \pm 0.014$	$69.44 \pm 0.018$
CIFAR-100C	$57.09 \pm 0.041$	$47.90 \pm 0.047$	$55.95 \pm 0.051$	$48.10 \pm 0.024$

### B.2 Analysis on parameter $K$

Table 9: Performance ( $Acc_{HM}$ ) on varying  $K$  with MNIST as strong OOD.

Weak OOD Dataset	# Classes	$K$					
		0	1	3	5	7	9
CIFAR-10C	10	80.97	83.9	84.32	84.17	84.10	84.02
ImageNet-R	200	64.32	83.65	83.87	83.53	83.39	83.42
ImageNet-C	1000	42.05	48.35	47.17	48.53	48.37	47.73

We vary the hyperparameter  $K$  which represents the number of positives and negatives chosen in Equation 6 and 7 and report the results ( $Acc_{HM}$ ) in Table 9. The size of the weak OOD feature bank  $\mathcal{M}_w$  is set as  $N_w = K \times C$ .  $N_s$  increases with the number of classes as well as the number of neighbours  $K$ . We set  $K$  to be 5 in all main results reported, which corresponds to feature bank size  $N_s$  of 50, 1000, 5000 respectively for the datasets CIFAR-10C, ImageNet-R and ImageNet-C respectively. In Table 9, we abuse the notion  $K = 0$  to correspond to the case where only  $\mathcal{L}_{PL}$  is used and no contrastive OOD loss is used. The results show that even with  $K = 1$ , there is a significant improvement in  $Acc_{HM}$  when compared to the case where  $\mathcal{L}_{OOD}^w, \mathcal{L}_{OOD}^s$  is not used ( $K = 0$ ). On further increasing  $K$ , we observe improvement only for the CIFAR-10C weak OOD dataset, but the performance is similar for ImageNet-R and ImageNet-C for higher values of  $K$  as well. Further, we investigate this observation that the performance of ROSITA is similar on significantly varying  $K$  or the feature bank size. For  $K = 5$ , we check the average number of positives actually selected for  $\mathcal{L}_{OOD}^w$  in Equation 6 for each of these datasets. We find this to be 4.1, 2.5 and 1.5 for CIFAR-10C, ImageNet-R and ImageNet-C respectively. This agrees with the results in Table 9 where  $K$  of 3, 5 works better compared to 1 as more neighbours have common pseudo label, aiding the clustering of classes of interest. For CIFAR-10C and ImageNet-R, using  $K < 5$  suffices and for ImageNet-C as only 1-2 neighbours are matched for majority of reliable OOD samples, setting  $K = 1$  suffices. For practical purposes, this observation suggests that the weak OOD feature buffer size can indeed be reduced based on storage budget available depending on the application and device the model is deployed on. For e.g., if the memory budget available can store only upto 1000 features,  $K$  can be set flexibly depending on the number of classes of interest. For ImageNet-C with 1000 classes,  $K$  can be set to 1.

### B.3 Loss Ablation

We provide detailed results of Table 4 including all the five metrics in Table 10. Additionally, we visualise the histograms of OOD scores on using different combinations of the proposed loss components in the Figures 6, 7, justifying their role in better discrimination of weak and strong OOD sample.

Table 10: Detailed results on Loss Ablation.

$\mathcal{L}_{PL}$	$\mathcal{L}_{OOD}^w$	$\mathcal{L}_{OOD}^s$	CIFAR-10C/MNIST					ImageNet-R/MNIST				
			AUC	FPR	$Acc_W$	$Acc_S$	$Acc_{HM}$	AUC	FPR	$Acc_W$	$Acc_S$	$Acc_{HM}$
✗	✗	✗	91.91	85.04	60.82	99.77	75.57	91.27	91.09	55.67	99.90	71.50
✓	✗	✗	95.29	30.82	68.36	99.30	80.97	81.07	99.02	48.42	95.76	64.32
✗	✓	✗	95.23	28.91	66.93	98.52	79.71	87.73	94.67	51.13	98.34	67.28
✗	✗	✓	98.61	12.73	66.60	99.68	79.84	99.39	4.81	67.81	99.99	80.82
✗	✓	✓	99.27	4.15	67.76	99.73	80.69	99.48	4.40	69.38	99.98	81.92
✓	✓	✓	99.10	7.63	72.81	99.74	84.17	99.44	4.29	71.73	99.98	83.53

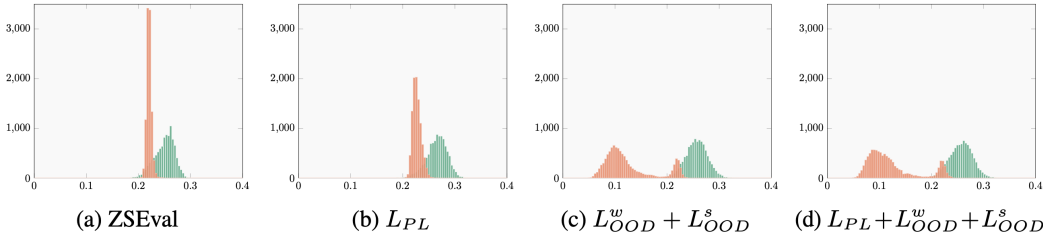


Figure 6: Histograms of Weak and Strong OOD scores for ZS-Eval and on using different loss components of ROSITA on CIFAR-10C/MNIST dataset using CLIP.

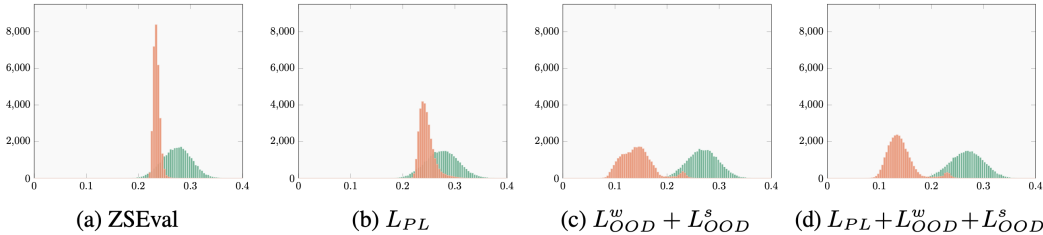


Figure 7: Histograms of Weak and Strong OOD scores for ZS-Eval and on using different loss components of ROSITA on ImageNet-R/MNIST dataset using CLIP.

From Figure 6 and 7, we observe that, on using just  $\mathcal{L}_{PL}$ , the weak and strong OOD scores still sufficiently overlap, similar to the case of ZSEval. The performance purely depends on the quality of pseudo labels of the detected reliable weak OOD samples. In CIFAR-10C, as there are only 10 classes and given that ZSEval performance in CIFAR-10C is fairly good, it ensures good quality pseudo labels, hence resulting in overall better metrics on even using  $\mathcal{L}_{PL}$  as shown in Table 10. ImageNet-R dataset inherently has more confusion as it is a 200-way classification problem. This naturally could result in low quality pseudo labels, in turn degrading the performance compared to ZSEval. Alongside, using  $\mathcal{L}_{PL}$  for weak OOD samples which are misclassified as strong OOD samples increases the FPR and results in a decrease in metrics overall compared to ZSEval. On the other hand, using  $\mathcal{L}_{OOD}^w + \mathcal{L}_{OOD}^s$  separates the OOD scores of weak and strong samples, resulting in two distinct peaks as seen in Figure 6 and 7, which in turn results in a significantly low FPR as reported in Table 10. The best results are obtained using all the three proposed loss components  $\mathcal{L}_{PL} + \mathcal{L}_{OOD}^w + \mathcal{L}_{OOD}^s$ , which better discriminates weak and strong OOD samples and also helps in selecting weak OOD samples with more accurate pseudo labels. Hence, using pseudo label loss and OOD contrastive losses aid each other, resulting in the best overall metrics as shown in Table 10.

#### B.4 Analysis on OOD Classifier and Reliable samples

Here, we study the role of OOD classifier in the Open World Single Image Test Time Adaptation setting. We compare the LDA based OOD classifier described in Section 3.1 in comparison with simple confidence thresholding with TTA algorithm of ROSITA described in 3.2. A test sample is classified as weak OOD if  $s_t^{ood} > \tau_t$  and strong OOD if  $s_t^{ood} < \tau_t$ . Further, in ROSITA, TTA is performed on reliable weak and strong OOD samples based on LDA statistics as described in Section 3.2. We generalize this and call a test sample as reliable weak OOD sample if  $s_t^{ood} > \tau_w$  and strong OOD if  $s_t^{ood} > \tau_s$ . Here, we perform experiments to understand the role of OOD classifier, reliable samples and the performance of ROSITA with time.

Table 11: Comparison of Simple threshold (row 1-3) vs LDA based OOD detector (row 5). Comparison of ROSITA using all samples (row 4) vs only reliable samples (row 5) for TTA.

Thresholds	strong OOD dataset: MNIST				
$\tau_s/\tau_t/\tau_w$	C-10C	C-100C	IN-C	IN-R	VisDA
0.4/0.6/0.8	43.44	34.42	1.20	77.12	88.49
0.3/0.5/0.7	33.70	32.60	1.74	80.29	50.87
0.5/0.5/0.5	22.82	37.41	1.91	30.90	32.31
$\tau_t/\tau_t/\tau_t$	<b>84.99</b>	55.16	44.05	83.28	<b>91.24</b>
$\mu_s/\tau_t/\mu_w$	84.17	<b>57.34</b>	<b>48.53</b>	<b>83.53</b>	90.64

**Effectiveness of the LDA based OOD classifier:** To study the role of the OOD classifier in ROSITA, we perform the following experiments **(1) Simple thresholding:** We set fixed thresholds  $\tau_w, \tau_s$  to identify reliable weak and strong OOD samples respectively and  $\tau_t$  to classify a sample into weak or strong OOD. **(2) LDA based:** As described in Section 3.1, we set  $\tau_w$  to  $\mu_w$  and  $\tau_s$  to  $\mu_s$  to identify reliable weak and strong OOD samples to perform TTA. We report the results ( $Acc_{HM}$ ) of all five weak OOD datasets with MNIST as strong OOD dataset using CLIP backbone. **Observations:** The first three rows in Table 11 correspond to simple thresholding cases where the thresholds are manually set and kept fixed throughout TTA using ROSITA. We observe that the performance significantly varies for different choice of thresholds, especially in the case of ImageNet-R (IN-R) and VisDA here. This shows that it is not feasible to choose these thresholds apriori in a TTA task as the softmax confidence scores depends on unknown factors like the type, severity of domain shift, confusion of classes etc. Hence, using fixed threshold to discriminate between weak and strong OOD samples is undesirable. In the OOD classifier we use (Section 3.1), a score bank  $\mathcal{S}$  is used to track how the OOD scores of the test samples change with time. The statistics  $\mu_w, \mu_s$  are continuously estimated to identify reliable weak and strong OOD samples. From Table 11, we observe that the best results (last row) are obtained on using the thresholds estimated in an online manner.

**Need for reliable samples:** To understand the role of selecting reliable samples for TTA, we do a simple experiment where we only use the threshold  $\tau_t$  to distinguish between a weak and strong OOD samples. For all weak OOD samples classified, we perform TTA using the loss defined in Equation 6. Similarly, we use the objective in Equation 7 for all strong OOD samples. The results are reported in the fourth row in Table 11. We see that, for CIFAR-10C and VisDA, this case performs slightly better than our case (last row in Table 11) where TTA is performed only on reliable samples. CIFAR-10C and VisDA dataset have 10 and 12 classes of interest respectively. The zero shot performance of these datasets being good, as the class confusion is less, using all samples for TTA can be helpful. On the other hand, the classification in CIFAR-100C, ImageNet-C and ImageNet-R is harder, due the confusion arising due to the large number of classes. Using non reliable test samples, with scores in the range  $\mu_s < s_t^{ood} < \mu_w$  can adversely affect the adaptation process. Hence, using only reliable samples for TTA performs better for these datasets as seen from the last two rows in Table 11). In a general test time adaptation scenario, where we have no prior information about the difficulty of the classification task, in terms of severity of domain shift and class confusion, it is desirable to only use reliable samples for model updates.

**Performance of ROSITA with time:** We plot the OOD scores of weak, strong OOD samples and the best threshold, with time in Figure 8a on using ROSITA. We observe that the OOD score



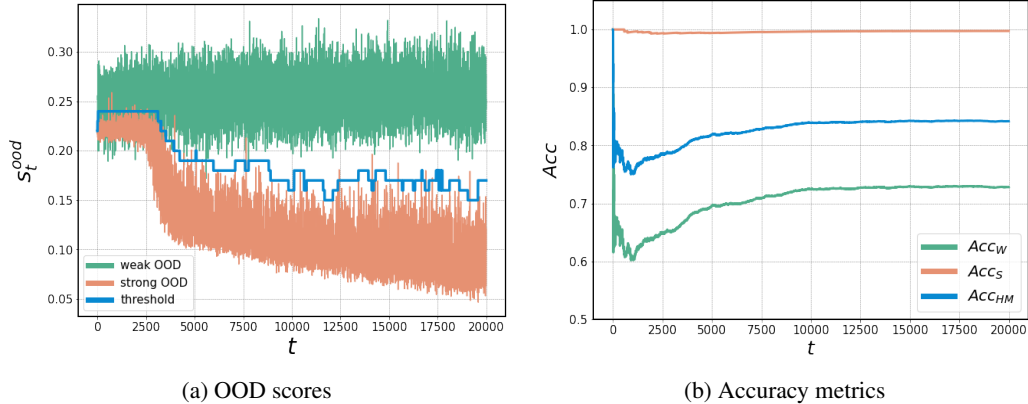


Figure 8: Analysis of ROSITA on CIFAR-10C/MNIST: (a) Change in OOD scores of **Weak** and **Strong** OOD samples, the best threshold with time  $t$ ; (b) Accuracy metrics  $Acc_W$ ,  $Acc_S$ ,  $Acc_{HM}$  measured for samples seen until time  $t$ . We see that the weak and strong OOD samples separate better with time. The accuracy metrics also improve with time.

values for weak and strong OOD samples become distinctive with time and the threshold estimated continuously tracks the changes in OOD scores. Better discrimination of weak and strong OOD samples aids the test time adaption process in ROSITA, resulting in a gradual improvement in the accuracy metrics as shown in Figure 8b. The metrics in Figure 8b are calculated based on the test samples seen until time  $t$ .

## B.5 Complexity Analysis

In addition to the complexity analysis presented on CLIP in Figure 4, here, in Figure 9, we plot the GPU memory required and the time taken (secs/image) for TTA on each dataset using MaPLE as the VLM backbone. The GPU memory and time taken scales with the number of classes for the prompt tuning baseline PAlign. However, in ROSITA, the computational complexity is comparable to the ZS-Eval case. The text classifiers are obtained once and kept fixed throughout the adaptation process as in ZS-Eval. In ROSITA, we perform a forward pass of the image and its augmentation and one backward pass if a sample is categorized as reliable weak or strong OOD.

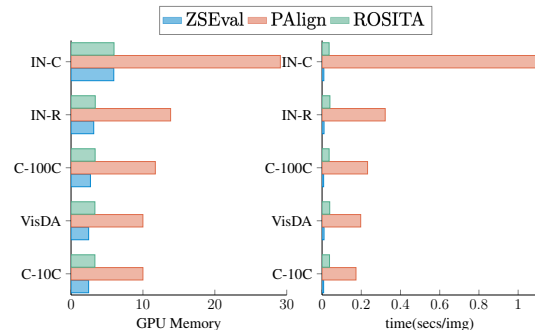


Figure 9: Complexity Analysis of different methods using MaPLE backbone.

**MaPLE backbone:** For ImageNet-C dataset with 1000 classes, ZSEval, PAlign and ROSITA require 5.94 GB, 29.12 GB and 5.98 GB GPU memory to perform a single image based model update. This makes the use of PAlign impractical and expensive for real time deployment in test scenarios, making it especially hard to port it on edge devices. The time taken to process a single image is 0.008s, 0.232s and 0.036s using ZSEval, PAlign and ROSITA respectively. This shows that ROSITA achieves the best trade off between memory and time complexity, being at par with ZSEval in terms of computational requirements while significantly outperforming ZSEval and the prompt tuning methods TPT and PAlign.

**Memory buffer:** While the baselines ZSEval, TPT, PAlign doesn't require any memory buffer, ROSITA requires a small memory buffer of size 512 for the OOD score bank and  $(C \times K + N_s) \times F$  for the feature banks. Here,  $C$ ,  $K$ ,  $N_s$  and  $F$  refer to the number of classes, number of neighbours, size of strong OOD feature bank and the feature dimension respectively. This memory buffer however enables significant improvement in the performance in the challenging single image openworld test time adaptation setting.

## C Additional Experiments

In addition to the results presented in the main paper, we perform additional experiments supporting the claims made and for more comprehensive understanding of the analysis presented in Section 5.

### C.1 Varying OOD ratio

In addition to the results presented in Table 6, we perform experiments using ImageNet-R weak OOD dataset which is a relatively large scale dataset with 50,000 images from 200 classes. We report the results on both the datasets and both CLIP and MaPLe backbone in Table 12. We observe consistent improvements compared to the baselines for both datasets of different scales.

Table 12: Results on varying OOD ratio.

		Ratio	CIFAR-10C/MNIST				IN-R/MNIST			
			0.2	0.3	0.6	0.8	0.2	0.3	0.6	0.8
CLIP	ZS-Eval	75.56	75.59	75.57	75.56	65.46	67.13	69.25	70.77	
	TPT	75.67	75.75	75.81	75.83	65.67	67.73	70.12	71.54	
	TPT-C	72.70	74.31	74.79	75.16	64.83	64.55	48.97	63.86	
	ROSITA	<b>82.96</b>	<b>83.97</b>	<b>84.51</b>	<b>84.37</b>	<b>82.22</b>	<b>83.32</b>	<b>83.59</b>	<b>83.84</b>	
MAPLE	ZS-Eval	80.47	80.67	81.21	82.21	68.88	71.13	73.45	74.02	
	PAlign	80.11	80.46	81.20	82.13	69.01	71.28	73.72	74.26	
	PAlign-C	80.93	83.10	83.58	83.83	71.99	73.85	74.65	74.72	
	ROSITA	<b>85.35</b>	<b>87.14</b>	<b>87.70</b>	<b>87.56</b>	<b>84.60</b>	<b>85.31</b>	<b>84.75</b>	<b>84.92</b>	

### C.2 Experiments using different corruption types

To evaluate the robustness of our method across different corruption types, we do additional experiments with *impulse noise*, *motion blur* and *jpeg compression* corruptions from the corruption categories per-pixel noise, blurring and digital transforms respectively and report the results here. From Table 13, Table 14 and Table 15, we observe that ROSITA either outperforms or at par with prior methods in most cases even on using the same set of hyperparameters. This demonstrates its robustness across a variety of corruption types.

Table 13: Results on CIFAR-10C/100C (Impulse Noise) with other strong OOD datasets.

		Method	MNIST			SVHN			Tiny-ImageNet			CIFAR-100C/10-C		
			AUC $\uparrow$	FPR $\downarrow$	HM $\uparrow$	AUC $\uparrow$	FPR $\downarrow$	HM $\uparrow$	AUC $\uparrow$	FPR $\downarrow$	HM $\uparrow$	AUC $\uparrow$	FPR $\downarrow$	HM $\uparrow$
-100C (Impulse noise)	CLIP	ZS-Eval	86.34	97.77	57.67	84.40	79.43	56.80	88.97	31.86	61.11	78.61	67.88	54.40
		TPT	86.35	97.83	59.80	84.43	79.52	58.97	88.96	31.99	64.48	78.60	68.24	56.38
		TPT-C	62.34	87.66	39.90	59.71	83.29	35.42	81.30	38.59	37.02	66.22	89.92	30.86
		ROSITA	98.87	9.43	71.31	82.85	56.82	61.03	93.36	21.47	64.47	78.69	69.45	57.87
-100C (Impulse noise)	MAPLE	ZS-Eval	91.10	76.09	64.01	92.98	45.28	63.66	83.77	44.44	60.93	79.22	65.26	57.49
		PAlign	91.10	76.01	65.76	93.00	45.13	65.28	83.78	44.42	62.75	79.22	65.24	58.80
		PAlign-C	92.43	63.39	63.61	92.92	45.86	64.50	83.36	45.74	60.83	79.30	64.47	57.00
		ROSITA	98.80	6.10	71.79	95.39	28.06	72.13	84.92	45.35	65.30	80.49	65.57	61.63
-100C (Impulse noise)	CLIP	ZS-Eval	70.48	99.17	25.08	51.12	96.44	25.69	59.90	67.18	27.72	53.51	94.97	25.16
		TPT	70.56	99.17	25.26	51.21	96.38	26.26	59.91	67.09	28.36	53.53	94.94	25.63
		TPT-C	57.65	93.07	8.71	79.28	57.07	2.74	90.40	22.60	5.71	50.26	95.34	3.26
		ROSITA	36.47	99.96	20.98	24.17	99.77	18.99	53.57	79.85	26.27	58.02	94.15	29.75
-100C (Impulse noise)	MAPLE	ZS-Eval	69.29	89.49	33.66	81.03	73.94	34.99	49.57	84.71	26.09	57.84	94.44	29.34
		PAlign	69.31	89.54	33.74	81.05	73.98	34.96	49.60	84.63	25.81	57.84	94.48	29.53
		PAlign-C	71.14	73.63	34.38	82.08	68.24	35.11	47.27	87.87	25.95	57.79	93.54	30.73
		ROSITA	95.38	8.80	43.06	80.25	41.21	34.88	42.77	97.15	19.70	49.73	96.72	12.62

Table 14: Results on CIFAR-10C/100C(Motion blur) with other strong OOD datasets.

	Method	MNIST			SVHN			Tiny-ImageNet			CIFAR-100C/10-C			
		AUC $\uparrow$	FPR $\downarrow$	HM $\uparrow$	AUC $\uparrow$	FPR $\downarrow$	HM $\uparrow$	AUC $\uparrow$	FPR $\downarrow$	HM $\uparrow$	AUC $\uparrow$	FPR $\downarrow$	HM $\uparrow$	
C-10C (Motion blur)	CLIP	ZS-Eval	97.73	2.75	73.69	96.40	18.34	73.82	95.25	15.75	74.27	79.57	70.08	62.86
		TPT	97.72	2.68	74.15	96.39	18.16	74.42	95.23	15.72	75.03	79.56	69.86	63.25
		TPT-C	80.73	86.28	63.74	62.09	62.52	42.19	80.76	51.66	48.04	55.66	97.04	37.53
	ROSITA	99.90	0.04	81.87	96.50	21.55	77.47	96.58	13.65	77.44	82.03	65.95	66.96	
	MAPLE	ZS-Eval	96.52	18.33	78.68	97.08	14.78	78.15	88.45	33.15	71.19	84.00	57.94	66.93
		PAlign	96.51	18.37	78.92	97.08	14.82	78.38	88.45	33.13	71.73	83.99	57.99	67.15
PAlign-C		97.17	13.47	78.49	96.89	15.87	78.09	88.80	32.94	72.09	84.29	56.80	67.40	
ROSITA	98.49	10.01	83.26	92.61	44.87	78.93	87.48	38.23	73.24	84.27	57.60	70.67		
C-100C (Motion blur)	CLIP	ZS-Eval	93.08	58.92	48.17	83.63	81.33	46.04	79.34	53.56	48.53	64.03	91.54	41.63
		TPT	93.06	59.87	48.18	83.61	81.56	45.54	79.29	53.76	48.26	64.02	91.63	41.25
		TPT-C	66.77	98.77	19.96	29.69	99.94	11.39	69.25	62.87	17.10	53.22	94.57	13.59
	ROSITA	98.93	6.79	55.49	89.39	37.86	48.50	90.20	31.61	55.05	65.30	91.59	42.54	
	MAPLE	ZS-Eval	81.21	80.28	45.66	89.04	60.73	46.98	60.84	80.63	40.60	64.01	90.18	42.30
		PAlign	81.20	80.52	44.52	89.03	61.01	45.76	60.84	80.64	40.03	64.01	90.26	41.26
PAlign-C		82.72	68.08	49.92	90.48	53.83	51.87	62.00	82.85	41.66	64.47	89.05	43.58	
ROSITA	97.12	7.78	57.30	85.13	56.16	49.89	63.85	80.20	42.65	62.55	94.62	41.54		

Table 15: Results on CIFAR-10C/100C(JPEG Compression) with other strong OOD datasets.

	Method	MNIST			SVHN			Tiny-ImageNet			CIFAR-100C/10-C			
		AUC $\uparrow$	FPR $\downarrow$	HM $\uparrow$	AUC $\uparrow$	FPR $\downarrow$	HM $\uparrow$	AUC $\uparrow$	FPR $\downarrow$	HM $\uparrow$	AUC $\uparrow$	FPR $\downarrow$	HM $\uparrow$	
C-10C (JPEG)	CLIP	ZS-Eval	68.16	100.00	53.92	67.04	99.93	55.69	79.44	65.02	59.66	73.65	85.60	56.30
		TPT	68.07	100.00	54.16	66.97	99.93	56.06	79.37	65.11	60.09	73.64	85.58	56.87
		TPT-C	68.28	99.37	53.12	54.76	98.97	35.64	66.70	72.20	39.02	59.82	94.78	32.78
	ROSITA	81.83	58.81	60.34	82.85	61.38	61.87	95.06	15.84	67.87	71.19	86.62	51.98	
	MAPLE	ZS-Eval	95.15	33.39	69.72	95.96	22.02	69.73	86.64	36.79	65.68	79.26	68.19	60.10
		PAlign	95.13	33.57	69.62	95.95	22.01	69.31	86.63	36.82	65.62	79.26	68.18	59.86
PAlign-C		96.53	20.14	70.50	95.94	21.51	70.01	87.38	35.07	66.42	79.85	66.17	61.11	
ROSITA	99.28	5.71	76.74	95.54	29.06	72.86	89.88	31.12	68.78	80.69	61.64	62.23		
C-100C (JPEG)	CLIP	ZS-Eval	50.88	100.00	32.27	39.25	100.00	26.41	48.65	95.60	29.92	53.51	95.59	32.48
		TPT	50.78	100.00	32.38	39.18	100.00	26.48	48.55	95.60	29.86	53.49	95.57	32.70
		TPT-C	12.11	100.00	3.32	10.05	99.98	2.45	63.07	90.01	9.49	52.23	95.05	6.33
	ROSITA	29.10	100.00	22.83	35.58	99.94	23.50	50.76	94.76	31.64	53.96	96.18	30.39	
	MAPLE	ZS-Eval	78.86	80.60	37.60	87.72	61.14	39.18	58.31	80.75	34.03	54.50	95.49	34.02
		PAlign	78.82	80.92	36.62	87.69	61.37	38.01	58.29	80.79	33.17	54.49	95.52	32.96
PAlign-C		81.85	63.37	40.87	89.96	49.09	41.89	59.33	81.48	33.84	53.82	95.17	33.28	
ROSITA	97.68	7.87	46.51	92.14	34.44	42.71	66.63	75.00	37.43	51.33	96.68	25.41		

### C.3 Experiments using CLIP ViT-B32 and CLIP ResNet50 architectures

To test the performance of ROSITA and prior methods across different architectures, we perform additional experiments using CLIP ViT-B/32 and CLIP ResNet50 models. In CLIP ResNet50 model, we finetune the BatchNorm parameters instead of LayerNorm. We observe that the performance improvement of ROSITA with respect to the baselines is agnostic to the model architecture of the VLM.

Table 16: Results on all datasets using CLIP ViT-B/32 and CLIP-ResNet50 architectures.

Method	MNIST			SVHN			Tiny-ImageNet			CIFAR-100C/10-C				
	AUC $\uparrow$	FPR $\downarrow$	HM $\uparrow$	AUC $\uparrow$	FPR $\downarrow$	HM $\uparrow$	AUC $\uparrow$	FPR $\downarrow$	HM $\uparrow$	AUC $\uparrow$	FPR $\downarrow$	HM $\uparrow$		
CIF <sub>r</sub> -100C	ViT-B/32	ZS-Eval	96.58	18.94	73.20	92.01	43.95	71.35	91.55	24.72	72.19	79.27	69.32	64.06
		TPT	96.55	19.44	73.96	91.97	44.31	71.96	91.54	24.81	73.61	79.25	69.48	64.59
		TPT-C	63.79	99.97	50.48	55.96	99.30	40.63	78.71	52.30	43.31	57.83	93.11	42.47
		ROSITA	99.14	3.84	81.65	93.78	33.45	75.18	98.86	4.14	80.91	80.28	64.17	64.34
RN50	ZS-Eval	36.73	100.00	31.49	59.79	99.07	41.01	84.64	36.21	54.61	67.63	87.30	45.19	
	TPT	37.26	100.00	32.18	60.25	99.03	41.95	84.76	36.07	56.41	67.62	87.37	45.98	
	TPT-C	14.06	98.57	5.46	36.98	93.76	19.11	73.60	62.60	22.87	51.23	91.64	19.69	
	ROSITA	62.45	99.87	47.63	96.30	23.90	65.52	96.51	11.03	59.34	68.30	83.64	49.11	
CIF <sub>r</sub> -100C	ViT-B/32	ZS-Eval	89.17	61.01	46.11	78.17	79.92	44.59	72.58	61.21	45.65	64.29	90.53	41.44
		TPT	89.08	61.15	45.99	78.06	80.11	44.78	72.57	61.24	46.25	64.31	90.47	41.65
		TPT-C	61.66	99.96	17.97	30.50	89.96	11.55	83.18	82.01	11.79	53.52	92.74	9.34
		ROSITA	94.34	23.99	57.14	90.26	45.33	51.60	91.22	30.17	56.02	68.33	86.03	44.57
RN50	ZS-Eval	23.47	100.00	14.27	37.73	99.91	20.84	65.59	61.52	27.77	54.28	94.77	22.18	
	TPT	23.88	100.00	14.17	38.18	99.91	20.49	65.80	61.22	27.39	54.30	94.82	21.81	
	TPT-C	24.35	97.90	2.32	13.57	99.96	2.44	83.84	44.88	4.17	53.54	95.29	3.84	
	ROSITA	23.73	100.00	15.27	66.59	73.78	28.34	73.04	60.32	26.57	54.30	93.50	23.52	

Table 17: Results with ImageNet-R/C as weak OOD, MNIST and SVHN as strong OOD datasets.

Method	IN-C/MNIST			IN-C/SVHN			IN-R/MNIST			IN-R/SVHN			
	AUC $\uparrow$	FPR $\downarrow$	HM $\uparrow$	AUC $\uparrow$	FPR $\downarrow$	HM $\uparrow$	AUC $\uparrow$	FPR $\downarrow$	HM $\uparrow$	AUC $\uparrow$	FPR $\downarrow$	HM $\uparrow$	
ViT-B/32	ZS-Eval	89.17	61.01	46.11	78.17	79.92	44.59	72.58	61.21	45.65	64.29	90.53	41.44
	TPT	89.08	61.15	45.99	78.06	80.11	44.78	72.57	61.24	46.25	64.31	90.47	41.65
	TPT-C	61.66	99.96	17.97	30.50	89.96	11.55	83.18	82.01	11.79	53.52	92.74	9.34
	ROSITA	94.34	23.99	57.14	90.26	45.33	51.60	91.22	30.17	56.02	68.33	86.03	44.57
RN50	ZS-Eval	91.15	61.44	17.56	92.37	43.01	19.23	87.39	98.23	57.87	92.34	55.18	60.40
	TPT	91.69	58.09	18.18	92.74	40.72	20.21	87.50	98.16	58.68	92.39	54.97	61.41
	TPT-C	95.00	10.45	1.74	29.09	99.98	1.31	71.95	97.61	37.79	75.25	78.47	41.85
	ROSITA	99.60	1.26	22.58	98.91	4.96	23.03	99.55	2.77	69.46	99.67	1.81	70.53

Table 18: Results with VisDA as weak OOD data.

Method	VisDA/MNIST			VisDA/SVHN			
	AUC $\uparrow$	FPR $\downarrow$	HM $\uparrow$	AUC $\uparrow$	FPR $\downarrow$	HM $\uparrow$	
ViT-B/32	ZS-Eval	89.10	95.57	73.85	85.54	80.62	71.93
	TPT	89.06	95.61	74.05	85.49	80.72	72.11
	TPT-C	66.98	99.75	62.89	17.01	99.83	13.62
	ROSITA	99.17	4.50	87.83	97.35	16.56	84.89
RN50	ZS-Eval	67.19	100.00	61.47	81.59	97.46	68.41
	TPT	67.28	100.00	61.60	81.60	97.43	68.62
	TPT-C	6.24	100.00	5.55	10.72	100.00	15.79
	ROSITA	78.57	99.96	66.89	98.44	8.06	79.87

### C.4 Open World Single Image CTTA Experiments

In addition to Table 5, we evaluate the performance of ROSITA in comparison with prior methods more extensively here. We present the 15 corruptions of CIFAR-10C sequentially, one sample at a time along with different strong OOD datasets, namely MNIST, SVHN, Tiny ImageNet, CIFAR-100C and report the results in Table 19. We observe that the improvement in performance of ROSITA is agnostic to model architecture, challenging scenarios including different combinations of weak (continuously changing domains) and strong OOD datasets.

Table 19: Results on Openworld Single Image Continuous Test Time Adaptation(CTTA) for CIFAR-10C (15 corruptions shown sequentially) as weak OOD dataset with four other strong OOD datasets.

Method		<i>gaussian</i>	<i>shot</i>	<i>impulse</i>	<i>defocus</i>	<i>glass</i>	<i>motion</i>	<i>zoom</i>	<i>snow</i>	<i>frost</i>	<i>fog</i>	<i>brightness</i>	<i>contrast</i>	<i>elastic</i>	<i>pixelate</i>	<i>jpeg</i>	Mean	
MNIST	CLIP	ZS-Eval	43.21	47.74	57.68	75.43	38.56	73.91	76.94	75.56	79.38	74.36	84.88	67.36	55.61	60.56	53.82	64.33
		TPT	43.15	47.66	<b>57.70</b>	75.36	38.22	73.70	76.84	75.49	79.32	74.80	84.82	67.46	55.50	60.40	53.48	64.26
		TPT-C	30.06	25.92	31.05	52.71	20.88	45.97	53.08	21.61	26.83	38.80	38.88	37.40	33.83	35.26	3.53	33.05
	ROSITA	<b>43.35</b>	<b>48.21</b>	57.04	<b>78.01</b>	<b>43.29</b>	<b>77.48</b>	<b>80.16</b>	<b>76.84</b>	<b>80.15</b>	<b>76.26</b>	<b>86.33</b>	<b>73.44</b>	<b>60.35</b>	<b>61.55</b>	<b>60.38</b>	<b>66.86</b>	
CIFAR-100	MAPLE	ZS-Eval	42.33	44.71	64.00	78.78	45.90	78.69	81.12	82.56	84.79	78.13	88.87	67.94	63.87	51.63	69.77	68.21
		PAlign	42.95	44.22	64.85	77.36	44.70	78.44	80.16	82.46	83.47	77.25	88.29	65.49	64.34	51.73	67.53	67.55
		PAlign-C	42.97	45.32	63.98	78.79	48.07	78.42	81.09	83.88	85.21	77.38	89.09	69.90	66.22	56.59	70.01	69.13
	ROSITA	<b>43.51</b>	<b>49.92</b>	<b>64.87</b>	<b>78.98</b>	<b>54.56</b>	<b>80.58</b>	<b>84.04</b>	<b>87.27</b>	<b>89.09</b>	<b>84.11</b>	<b>93.02</b>	<b>78.60</b>	<b>74.02</b>	<b>71.64</b>	<b>75.30</b>	<b>73.97</b>	
SVHN	CLIP	ZS-Eval	42.86	47.15	56.79	75.11	41.57	74.03	76.65	74.07	77.73	73.66	83.01	68.03	54.80	59.66	55.58	64.05
		TPT	42.82	47.10	56.82	74.98	41.49	73.88	76.64	74.05	77.67	73.93	82.95	68.32	54.70	59.60	55.51	64.03
		TPT-C	37.26	34.53	39.45	62.23	30.72	55.30	62.65	45.74	47.70	50.35	55.42	57.01	43.26	45.32	29.64	46.44
	ROSITA	<b>43.08</b>	<b>47.99</b>	<b>57.62</b>	<b>76.73</b>	<b>42.35</b>	<b>74.99</b>	<b>78.59</b>	<b>76.34</b>	<b>78.54</b>	<b>72.00</b>	<b>83.58</b>	<b>68.93</b>	<b>60.21</b>	<b>60.08</b>	<b>57.86</b>	<b>65.26</b>	
CIFAR-10	MAPLE	ZS-Eval	45.34	50.19	63.65	78.24	52.00	78.13	80.62	83.57	85.00	77.77	88.80	67.55	63.51	55.23	69.73	69.29
		PAlign	<b>45.74</b>	50.29	64.35	76.99	51.50	77.97	79.89	83.16	83.63	76.89	88.47	65.56	64.10	55.91	67.70	68.81
		PAlign-C	45.36	50.36	63.83	78.19	51.55	77.84	80.50	83.05	84.42	76.82	88.15	71.57	65.50	55.01	70.04	69.48
	ROSITA	45.51	<b>50.99</b>	<b>64.73</b>	<b>78.36</b>	<b>53.10</b>	<b>78.74</b>	<b>80.87</b>	<b>83.79</b>	<b>85.18</b>	<b>78.47</b>	<b>88.71</b>	<b>70.78</b>	<b>66.70</b>	<b>59.28</b>	<b>71.18</b>	<b>70.43</b>	
Tiny	CLIP	ZS-Eval	49.41	52.96	61.09	76.40	49.23	74.28	77.36	74.49	77.39	73.92	81.34	70.26	60.29	59.40	59.67	66.50
		TPT	49.43	52.97	61.07	76.41	49.13	74.27	77.36	74.63	77.43	74.05	81.49	70.14	60.16	59.28	59.66	66.50
		TPT-C	49.64	51.56	59.10	74.35	47.37	66.65	71.56	60.46	62.19	63.91	69.60	63.85	55.65	52.31	42.58	59.38
	ROSITA	<b>49.64</b>	<b>53.56</b>	<b>61.64</b>	<b>77.02</b>	<b>50.23</b>	<b>76.09</b>	<b>79.22</b>	<b>78.05</b>	<b>79.34</b>	<b>76.84</b>	<b>84.55</b>	<b>73.65</b>	<b>65.87</b>	<b>58.86</b>	<b>68.76</b>	<b>68.89</b>	
CIFAR-100	MAPLE	ZS-Eval	44.18	47.30	60.94	71.71	49.99	71.18	73.40	76.15	76.76	71.56	80.22	64.44	61.51	55.67	65.69	64.71
		PAlign	44.17	46.35	61.56	70.27	48.90	70.63	72.46	75.57	75.32	70.66	79.65	62.53	62.15	56.28	63.13	63.98
		PAlign-C	<b>44.38</b>	<b>48.00</b>	61.09	72.15	49.94	72.06	74.47	76.10	<b>77.67</b>	72.13	80.51	66.68	61.75	55.69	66.51	65.28
	ROSITA	44.29	47.93	<b>61.59</b>	<b>72.35</b>	<b>51.11</b>	<b>72.20</b>	<b>74.47</b>	<b>76.34</b>	77.45	<b>72.89</b>	<b>80.82</b>	<b>66.70</b>	<b>62.81</b>	<b>57.72</b>	<b>67.00</b>	<b>65.71</b>	
CIFAR-100	CLIP	ZS-Eval	40.48	44.50	54.34	67.17	40.46	62.85	68.16	68.90	70.68	65.22	76.26	62.16	51.48	48.42	56.23	58.49
		TPT	40.43	44.45	54.32	67.13	40.40	62.89	68.14	68.90	70.71	65.17	76.24	62.13	51.41	48.46	56.31	58.47
		TPT-C	27.80	26.46	33.01	40.72	28.05	38.78	42.05	41.90	43.91	39.15	45.80	41.50	37.11	32.71	39.69	37.24
	ROSITA	<b>40.66</b>	<b>45.15</b>	<b>55.01</b>	<b>67.31</b>	<b>41.07</b>	<b>63.12</b>	<b>68.54</b>	<b>69.58</b>	<b>71.09</b>	<b>66.23</b>	<b>76.34</b>	<b>63.89</b>	<b>54.15</b>	<b>48.23</b>	<b>57.08</b>	<b>59.16</b>	
CIFAR-100	MAPLE	ZS-Eval	41.99	45.82	57.50	69.19	44.03	66.86	70.43	<b>71.81</b>	<b>73.33</b>	68.32	76.95	64.18	56.74	49.81	60.15	61.14
		PAlign	41.93	45.16	57.81	68.04	42.44	66.54	69.56	71.35	71.78	67.46	76.70	62.17	56.98	49.86	58.22	60.40
		PAlign-C	41.86	45.80	57.51	69.78	46.17	<b>67.73</b>	<b>71.47</b>	71.03	74.00	68.98	77.61	65.53	57.08	52.17	61.17	61.86
	ROSITA	<b>42.13</b>	<b>46.09</b>	<b>58.00</b>	<b>69.48</b>	<b>45.33</b>	67.44	71.00	71.00	73.31	<b>69.42</b>	<b>78.37</b>	<b>65.55</b>	<b>57.32</b>	<b>53.52</b>	<b>60.85</b>	<b>61.92</b>	

## D Detailed Experimental Results

Here, we report in detail all the metrics (Section 3.2), namely AUC, FPR,  $Acc_W$ ,  $Acc_S$ ,  $Acc_{HM}$  of the main tables Table 1, Table 2, Table 3.

Table 20: Detailed results using CIFAR-10C as weak OOD with other strong OOD datasets.

Method		CIFAR-10C/MNIST					CIFAR-10C/SVHN				
		AUC	FPR	$Acc_W$	$Acc_S$	$Acc_{HM}$	AUC	FPR	$Acc_W$	$Acc_S$	$Acc_{HM}$
CLIP	ZS-Eval	91.91	85.04	60.82	99.77	75.57	89.93	64.20	60.82	94.74	74.08
	TPT	91.89	85.55	61.13	99.78	75.81	89.93	64.41	61.16	94.83	74.36
	TPT-C	81.64	67.53	59.88	<b>99.82</b>	74.86	58.48	71.72	37.11	69.00	48.26
	ROSITA	<b>99.10</b>	<b>7.63</b>	<b>72.81</b>	99.74	<b>84.17</b>	<b>94.79</b>	<b>32.59</b>	<b>66.64</b>	<b>96.40</b>	<b>78.80</b>
MAPLE	ZS-Eval	98.48	3.77	72.08	99.60	83.63	<b>98.34</b>	<b>7.86</b>	73.08	97.58	83.57
	TPT	98.15	5.67	69.04	99.64	81.56	98.34	7.89	71.78	97.63	82.73
	TPT-C	98.56	<b>3.74</b>	71.87	99.64	83.51	98.32	8.18	72.76	97.87	83.47
	PAlign	98.15	5.67	70.02	99.64	82.24	98.34	7.90	72.95	97.64	83.51
	PAlign-C	98.56	3.74	71.84	99.65	83.49	98.32	8.13	<b>78.71</b>	97.89	83.46
	ROSITA	<b>99.34</b>	5.22	<b>78.02</b>	<b>99.93</b>	<b>87.63</b>	97.80	13.15	73.49	<b>98.49</b>	<b>84.17</b>

Method		CIFAR-10C/Tiny					CIFAR-10C/CIFAR-100C				
		AUC	FPR	$Acc_W$	$Acc_S$	$Acc_{HM}$	AUC	FPR	$Acc_W$	$Acc_S$	$Acc_{HM}$
CLIP	ZS-Eval	91.33	27.07	70.55	79.20	74.63	82.57	67.92	60.81	79.45	68.89
	TPT	91.31	27.23	71.55	79.17	75.17	82.57	68.06	61.15	<b>79.61</b>	69.17
	TPT-C	74.08	61.45	37.65	73.89	49.88	61.45	94.30	34.54	69.31	46.10
	ROSITA	<b>96.43</b>	<b>12.10</b>	<b>74.81</b>	<b>86.11</b>	<b>80.06</b>	<b>82.99</b>	<b>62.89</b>	<b>66.63</b>	72.75	<b>69.56</b>
MAPLE	ZS-Eval	90.86	27.54	74.49	77.66	76.04	86.14	<b>52.08</b>	67.99	75.97	71.76
	TPT	90.86	27.61	73.47	77.56	75.46	86.15	52.14	66.61	<b>75.87</b>	70.94
	TPT-C	91.18	26.93	75.27	77.37	76.31	86.50	50.56	70.59	71.56	71.07
	PAlign	90.86	27.60	74.49	77.53	75.98	86.15	52.18	67.65	75.85	71.52
	PAlign-C	91.18	26.90	75.28	77.35	76.30	86.50	50.58	70.58	71.51	71.04
	ROSITA	<b>91.67</b>	<b>25.31</b>	<b>76.69</b>	<b>78.67</b>	<b>77.67</b>	<b>86.82</b>	50.33	<b>72.96</b>	73.35	<b>73.15</b>

Table 21: Detailed results using ImageNet-C as weak OOD with MNIST/SVHN as strong OOD.

Method		ImageNet-C/MNIST					ImageNet-C/SVHN				
		AUC	FPR	$Acc_W$	$Acc_S$	$Acc_{HM}$	AUC	FPR	$Acc_W$	$Acc_S$	$Acc_{HM}$
CLIP	ZS-Eval	93.39	55.52	26.14	99.89	41.43	85.89	72.91	26.10	93.78	40.83
	TPT	93.12	58.01	26.76	99.88	42.21	85.43	74.47	26.18	94.03	40.95
	TPT-C	56.57	99.12	3.25	62.57	6.19	11.38	100.00	4.03	35.16	7.24
	ROSITA	<b>99.52</b>	<b>4.06</b>	<b>32.04</b>	<b>99.97</b>	<b>48.53</b>	<b>98.34</b>	<b>10.21</b>	<b>30.21</b>	<b>99.21</b>	<b>46.32</b>
MAPLE	ZS-Eval	81.49	92.95	26.60	96.40	41.70	83.26	71.15	28.06	89.81	42.77
	TPT	81.38	93.17	25.17	96.33	39.92	83.18	71.52	26.50	89.93	40.93
	TPT-C	83.25	87.60	27.55	95.96	42.81	83.18	70.60	28.28	88.49	42.86
	PAlign	81.38	93.17	26.30	96.33	41.32	83.18	71.52	27.65	89.93	42.30
	PAlign-C	71.22	86.32	16.78	70.89	27.14	32.17	94.32	10.36	30.29	15.44
	ROSITA	<b>99.56</b>	<b>1.66</b>	<b>34.50</b>	<b>99.92</b>	<b>51.30</b>	<b>98.68</b>	<b>5.09</b>	<b>34.05</b>	<b>98.95</b>	<b>50.67</b>

Table 22: Detailed results using CIFAR-100C as weak OOD with other strong OOD datasets.

Method	CIFAR-100C/MNIST					CIFAR-100C/SVHN					
	AUC	FPR	$Acc_W$	$Acc_S$	$Acc_{HM}$	AUC	FPR	$Acc_W$	$Acc_S$	$Acc_{HM}$	
CLIP	ZS-Eval	77.78	99.93	32.05	<b>98.68</b>	48.39	64.70	98.68	32.05	80.55	45.85
	TPT	77.76	99.94	32.00	98.72	48.33	64.71	98.63	32.00	80.85	45.85
	TPT-C	51.57	100.00	17.51	59.31	27.04	9.40	99.98	3.62	13.90	5.74
	<b>ROSITA</b>	<b>96.07</b>	<b>19.28</b>	<b>40.63</b>	97.41	<b>57.34</b>	<b>82.09</b>	<b>64.64</b>	<b>32.59</b>	<b>92.32</b>	<b>48.17</b>
MAPLE	ZS-Eval	87.43	64.19	38.73	94.69	54.97	92.98	40.51	39.54	98.45	56.42
	TPT	87.42	64.09	36.89	94.68	53.09	92.97	40.44	37.55	98.48	54.37
	TPT-C	87.65	63.08	38.90	94.68	55.14	93.09	40.30	39.43	98.49	56.31
	PAlign	87.42	64.11	37.75	94.68	53.98	92.97	40.48	38.51	98.48	55.37
	PAlign-C	88.25	57.31	39.75	92.99	55.69	93.45	39.39	40.58	97.95	57.39
	<b>ROSITA</b>	<b>97.04</b>	<b>11.01</b>	<b>45.11</b>	<b>99.41</b>	<b>62.06</b>	<b>96.26</b>	<b>20.99</b>	<b>42.30</b>	<b>98.89</b>	<b>59.25</b>

Method	CIFAR-100C/Tiny					CIFAR-100C/CIFAR-10C					
	AUC	FPR	$Acc_W$	$Acc_S$	$Acc_{HM}$	AUC	FPR	$Acc_W$	$Acc_S$	$Acc_{HM}$	
CLIP	ZS-Eval	67.31	73.89	35.35	65.01	45.80	63.28	93.25	32.04	70.42	44.04
	TPT	67.28	73.82	35.55	64.88	45.93	63.26	93.20	31.99	70.57	44.02
	TPT-C	59.74	79.76	10.68	66.75	18.41	55.86	<b>86.35</b>	7.64	63.33	13.64
	<b>ROSITA</b>	<b>83.55</b>	<b>50.76</b>	<b>45.69</b>	<b>71.91</b>	<b>55.88</b>	<b>68.54</b>	89.71	<b>36.92</b>	<b>68.52</b>	<b>47.98</b>
MAPLE	ZS-Eval	68.80	74.35	38.44	64.74	48.24	66.93	87.94	33.45	73.94	46.06
	TPT	68.80	<b>74.20</b>	36.88	64.65	46.97	66.93	87.95	31.75	73.71	44.38
	TPT-C	68.85	74.71	38.84	64.67	48.53	66.97	87.94	34.01	72.48	46.30
	PAlign	68.80	74.23	<b>37.78</b>	64.64	47.69	66.93	87.93	32.56	73.66	45.16
	PAlign-C	68.76	78.12	37.31	67.87	48.15	66.82	87.80	35.72	<b>68.74</b>	47.01
	<b>ROSITA</b>	<b>70.37</b>	77.00	37.62	<b>68.97</b>	<b>48.68</b>	<b>69.57</b>	<b>83.61</b>	<b>38.03</b>	68.09	<b>48.80</b>

Table 23: Detailed results using ImageNet-R as weak OOD with MNIST/SVHN as strong OOD.

Method	ImageNet-R/MNIST					ImageNet-R/SVHN					
	AUC	FPR	$Acc_W$	$Acc_S$	$Acc_{HM}$	AUC	FPR	$Acc_W$	$Acc_S$	$Acc_{HM}$	
CLIP	ZS-Eval	91.27	91.09	55.67	99.90	71.50	90.43	75.04	56.36	98.38	71.66
	TPT	91.25	91.23	56.26	99.90	71.98	90.43	74.98	57.22	98.40	72.36
	TPT-C	82.81	85.79	51.86	99.78	68.25	80.94	80.03	54.88	93.55	69.18
	<b>ROSITA</b>	<b>99.44</b>	<b>4.29</b>	<b>71.73</b>	<b>99.99</b>	<b>83.53</b>	<b>98.62</b>	<b>9.08</b>	<b>67.90</b>	<b>99.61</b>	<b>80.75</b>
MAPLE	ZS-Eval	90.15	83.54	59.79	98.51	74.42	92.74	65.70	61.20	99.24	75.71
	TPT	90.14	83.58	59.26	98.51	74.00	92.74	65.68	60.56	99.26	75.23
	TPT-C	90.35	81.49	60.20	98.52	74.73	92.79	65.20	61.03	99.26	75.59
	PAlign	90.14	83.58	60.11	98.51	74.66	92.74	65.68	61.48	99.26	75.93
	PAlign-C	92.20	59.70	60.72	98.88	75.23	93.54	54.59	61.12	99.33	75.67
	<b>ROSITA</b>	<b>99.39</b>	<b>2.95</b>	<b>73.49</b>	<b>99.96</b>	<b>84.70</b>	<b>97.85</b>	<b>12.98</b>	<b>71.14</b>	<b>99.80</b>	<b>83.07</b>

Table 24: Detailed results using VisDA as weak OOD with MNIST/SVHN as strong OOD.

	Method	VisDA/MNIST					VisDA/SVHN				
		AUC	FPR	$Acc_W$	$Acc_S$	$Acc_{HM}$	AUC	FPR	$Acc_W$	$Acc_S$	$Acc_{HM}$
CLIP	ZS-Eval	93.55	65.88	64.35	99.92	78.28	90.46	65.03	64.32	96.00	77.03
	TPT	93.56	66.04	64.53	99.92	78.42	90.47	65.05	64.59	96.06	77.24
	TPT-C	81.84	86.12	60.52	99.79	75.35	81.24	91.32	55.87	94.96	70.35
	<b>ROSITA</b>	<b>99.59</b>	<b>3.26</b>	<b>82.92</b>	<b>99.94</b>	<b>90.64</b>	<b>98.89</b>	<b>6.48</b>	<b>80.53</b>	<b>99.76</b>	<b>89.12</b>
MAPLE	ZS-Eval	93.07	66.00	67.35	99.23	80.24	94.41	40.56	67.35	99.13	80.21
	TPT	93.07	66.11	67.45	99.24	80.31	94.41	40.51	67.45	99.15	80.28
	TPT-C	95.67	27.45	69.79	99.54	82.05	94.53	38.87	67.43	99.16	80.28
	PAlign	93.07	66.11	67.89	99.24	80.63	94.41	40.51	67.92	99.15	80.61
	PAlign-C	95.60	27.97	69.61	99.53	81.92	95.67	26.87	70.09	98.95	82.06
	<b>ROSITA</b>	<b>99.80</b>	<b>1.41</b>	<b>83.21</b>	<b>99.99</b>	<b>90.83</b>	<b>98.87</b>	<b>6.48</b>	<b>81.33</b>	<b>99.94</b>	<b>89.68</b>